on an empirical correlation of wing tunnel data on the effects of tip shape (Reference 2). It is estimated that the tip curvature of 401B reduces the minimum drag coefficient by .0005 at subsonic speeds and by .0015 at supersonic speeds. These are the increments applied to the form and wave drag components, respectively, in the minimum drag buildup.

(U) The remaining increments in the above equation require special treatment and are discussed in the following paragraphs. The incremental minimum drag variations with Mach number for the effects of canopy, nozzle, diverter, cowl, secondary systems, missile pylons, and protuberances are plotted in Figures 3.3-2.

(U) Canopy. The canopy drag is derived from Convair FX wind tunnel test C.A.L. 316-133. The test canopy is similar to the canopy on Configuration 401B. As a result, the 401B canopy D/q is obtained from the test data by ratioing the canopy frontal areas and then basing the drag coefficient on the 401B wing reference area.

(U) Nozzle. The reference nozzle drag is the boattail pressure drag on the installed nozzle. An average maximum-power nozzle position (40-inch exit diameter) was used as the reference nozzle position for all (both subsonic and supersonic) calculations of the reference nozzle drag. Variations in nozzle drag due to engine power setting are included in the thrust. Reference nozzle drag is estimated by use of the "Revised McDonald-Hughes Method," as described in Reference 3. Additional discussion of the nozzle drag is given in Section 3.6.

(U) Diverter. This drag increment is the pressure drag on the inlet boundary-layer diverter. It is determined from a computation of the average wedge pressure coefficient accounting for the total pressure loss through the boundary layer, when significant.

(U) Cowl. This drag increment accounts for the compression due to the locally high slopes in the first 30 inches of the inlet cowl when operating at a A_o/A_I of 1.0 (the basic drag equation applies at $A_o/A_I = 1.0$ only). A second-order shock-expansion method applicable to bodies of revolution (Reference 4) was used to predict this increment. Cowl drag variation with reduced A_o/A_I are included in the propulsion data (Section 3.6).

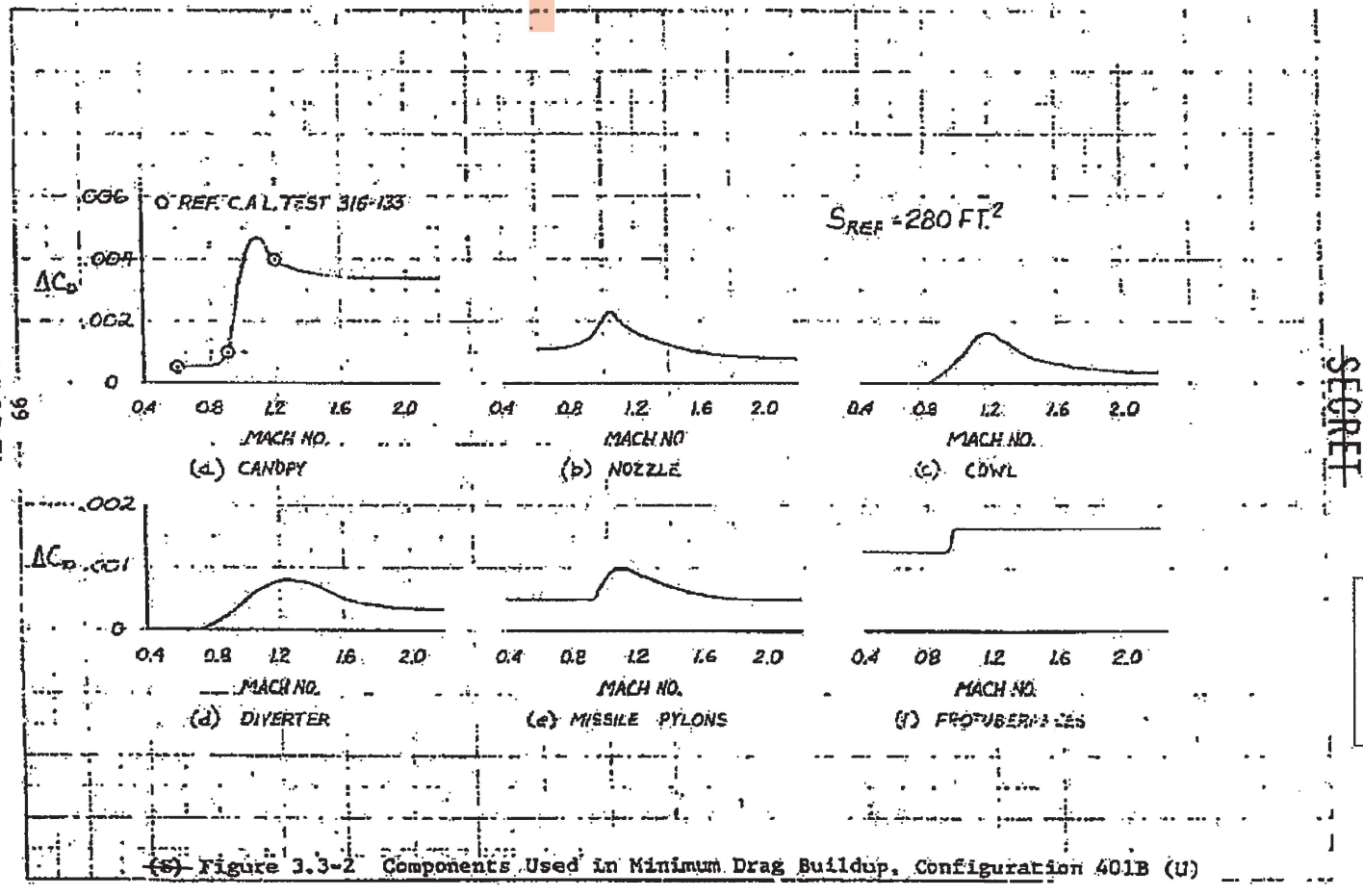

(S) Figure 3.3-2 Components Used in Minimum Drag Buildup, Configuration 401B (U)

(U) Secondary Systems. This drag increment accounts for momentun losses due to the aircraft auxiliary air systems. These systems encompass all functions, other than the engine, requiring external air. Included are the ECS ram-air system, the gun-compartment purging system, the oil-cooler air system, and the engine-compartment air system. The drag coefficient increment applied for these systems on 401B is .0002 at both subsonic and supersonic speeds. A momentun-loss analysis for the secondary-air system is the basis for this estimate. Additional discussion is provided in Section 3.6.

(U) Missile Pylons. This drag increment accounts for the two AIM-9X missile pylons. It is based on test data reported in References 5 and 6 adjusted for pylon size differences.

(U) Protuberances. This is an estimate of the drag due to antennae, air-data probes, ram-air scoops, navigation lights, and static dischargers. This drag term is based on data provided in Reference 7.

3.3.1.2 External Store Drag

(U) The external store drags used in mission performance calculations are shown in Figure 3.3-3. The increments are derived from F-111 test data documented in References 5 and 6.

3.3.1.3 Airplane Growth Effects

(U) The variation of minimum drag drag coefficient with aircraft size (gross weight) at constant wing loading is presented in Figure 3.3-4. The basic form and friction drag were computed for two other gross-weight airplanes, 15,600 and 18,000 lb. Canopy, nozzle, cowl, diverter, secondary systems, missile pylons and protuberances are assumed to have constant D/q, (i.e., are constant size and independent of airplane size). Also, it is assumed that the ratio of tail and ventral area to wing area is approximately independent of airplane size, and, therefore, the wave drag coefficient of the wing, tails, and ventrals is constant. The fuselage wave drag coefficient (based on frontal area) is considered to be inversely proportional to the square of the fineness ratio; therefore,

$$\left(C_{D_{wave}}\right)_{fuselage} \propto \frac{1}{FR^2} \left(\frac{A_{frontal}}{S_{ref}}\right)$$

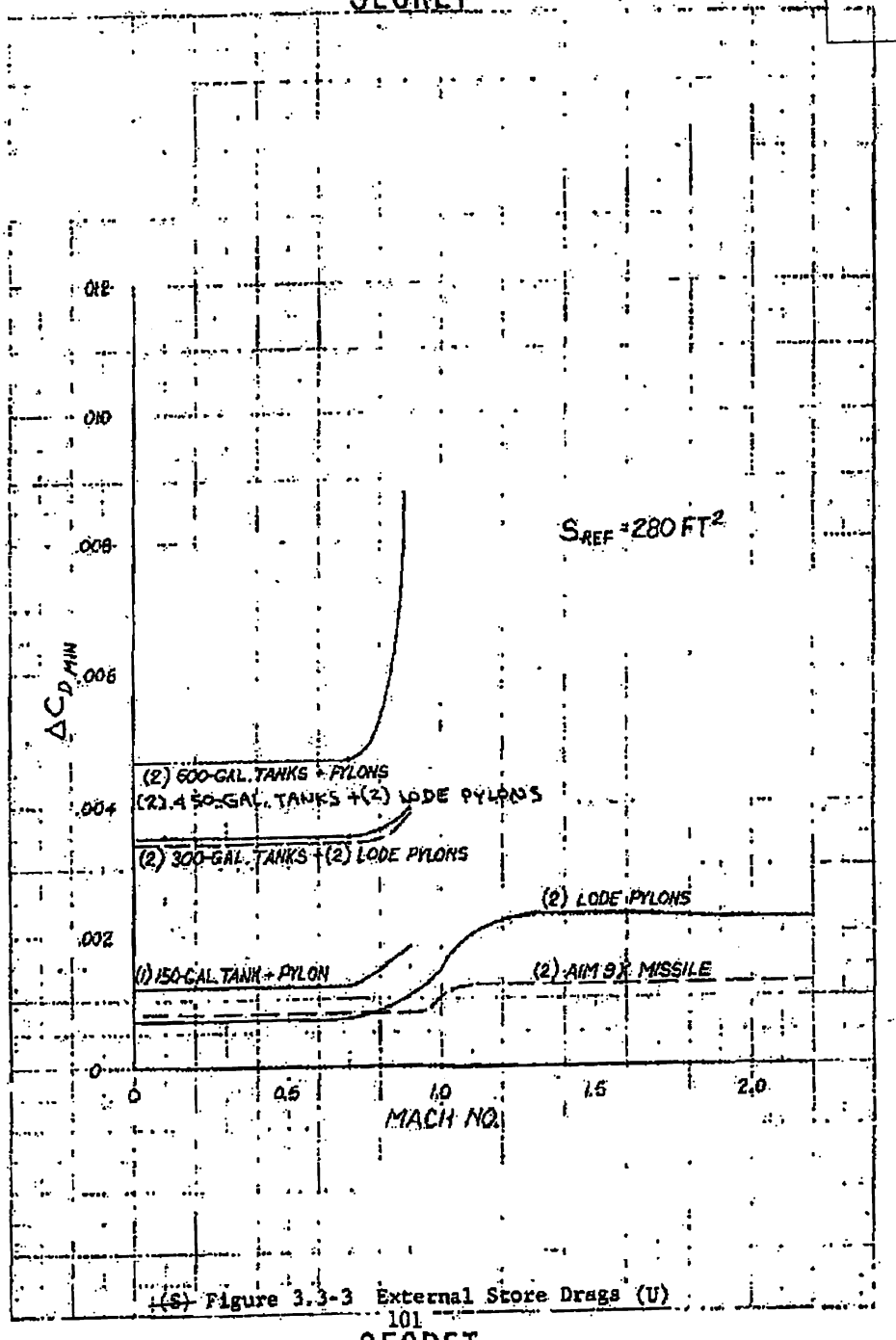

(S) Figure 3.3-3 External Store Drags (U)

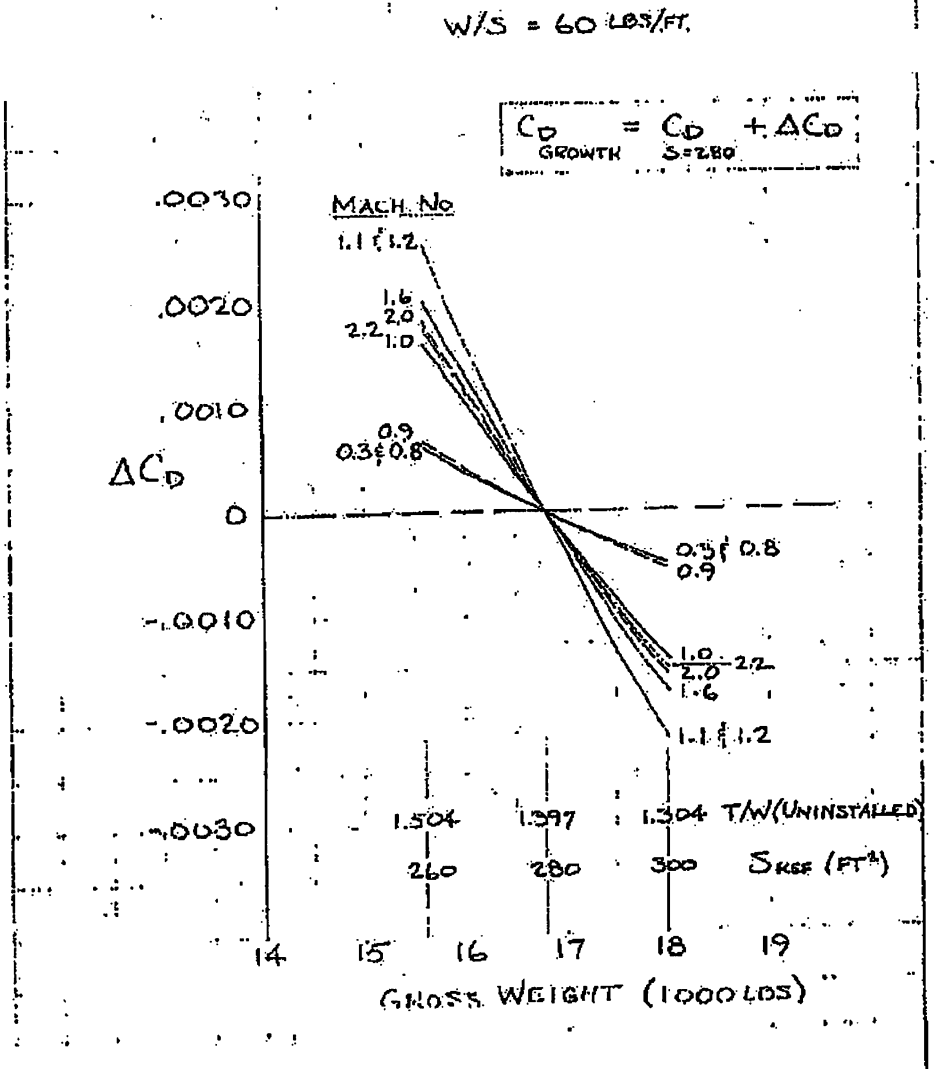

~~(S)~~ Figure 3.3-4 Effect of Aircraft Size on Minimum Drag Coefficient, Configuration 401B (U)

(U) If an estimate of the length and frontal area variation with aircraft size is given, the variation of fuselage wave drag can be computed.

~~(S)~~ The minimum drag presented above in Subsection 3.3.1.1 is for the initial design gross weight of 16,800 lb. The final gross weight required for mission performance is slightly higher, 17,115 lb, and the minimum drag can be adjusted accordingly from the data of Figure 3.3-4.

3.3.2 Drag Due to Lift

(U) The drag polar shape, including the effects of leading-edge flaps, are based on Convair Aerospace FX wind tunnel tests at the Cornell Aeronautical Laboratory (C.A.L. Test 316-113 and C.A.L. Test G52-423). The validity of this data for application to Configuration 401B is readily seen in Figure 3.3-5, where the planforms of the FX-132 wind tunnel model and Configuration 401B are compared.

(U) The leading-edge-flap design on the wind tunnel model has

$$C_f/C = 18\% \text{ at the root}$$

and

$$C_f/C = 30\% \text{ at the tip}$$

This is identical to the leading-edge maneuver flap designed for Configuration 401B.

The only adjustments made to the test data are

1. An aspect ratio correction of 3.0 to 3.2.
2. A t/c correction of .035 to .040.

(U) The drag-due-to-lift polars are presented for specific Mach numbers at the pertinent leading edge flap settings in in Figures 3.3-6 through 3.3-10. The minimum-drag increment due to leading-edge flap deflection is defined in Figure 3.3-11.

3.3.3 Trim Drag

(U) Trim drag is defined to be the drag increment at constant C_L between the $\delta_H = 0$ polar and the $\delta_H = \delta_{H_{trim}}$ polar as shown by the sketch below.

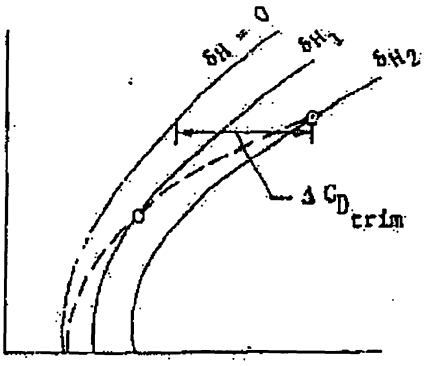

(U) The longitudinal stability characteristics and horizontal tail deflections required to trim are discussed in Section 3.4. These required deflections at various pertinent flight conditions are plotted in Figure 3.3-12.

(U) The estimated drag due to these deflections, shown in Figure 3.3-13, is based on wind tunnel data (from C.A.L. Test G52-423) for an FX-132 configuration with an aspect ratio 3.0 planform, differing only slightly ($\Lambda = 31.5^{\circ}$ instead of 35°, $\lambda = 0.3$ instead of 0.2) from the one shown in Figure 3.3-5. The airfoil (.035 biconvex) and leading-edge flap are identical.

(U) As indicated in Figures 3.3-12 and -13 all performance calculations are made for a center of gravity of 27% MAC, which was selected to provide a minimum of 3% static margin within the combat envelope.

3.3.4 Trimmed Drag Polars

(U) The trimmed drag polars used in the performance calculations are shown in Figures 3.3-14 through 3.3-19. The high C_L drag polars used for the energy-maneuverability plots are given in Figure 3.3-18. The trimmed drag polars used in takeoff and landing calculations are given in 3.3-19. In Figures 3.3-20 through 3.3-24, the same data are plotted on the basis of $C_L/(W/S)$ versus $C_D/(W/S)$.

(U) Trimmed $(L/D)_{max}$ versus Mach number is presented in Figure 3.3-25 for various leading-edge flap deflections. It is seen that the leading-edge flap design of Configuration 401B is a very effective cambering device. A deflection of 10 degrees increases the $(L/D)_{max}$ by 20 percent, to 10.8. This is only about 12 percent less than the $(L/D)_{max}$ expected for a blunt-nosed cambered airfoil, and the variable flap eliminates the off-design penalties associated with fixed camber.

3.3.5 Lift and Buffet Characteristics

(U) Trimmed and untrimmed C_L-vs-α curves for Configuration 401B are shown in Figures 3.3-26 through 3.3-29. The trimmed C_L-vs-α curves for takeoff and landing are shown in Figure 3.3-30. These lift predictions are based on C_L-vs-α and C_L-vs-δ_H from C.A.L. Test G52-423 mentioned earlier.

(U) The method used for predicting buffet characteristics is based on an analysis of the C_L-vs-α curves in the non-linear region. This method has been checked through comparison with available flight data, and reasonable agreement has been obtained. Derivation and documentation of the method is contained in Reference 8.

(U) The following boundaries are defined in terms of predicted flight buffet acceleration:

buffet onset: $\Delta n_B = \pm .05g$

moderate buffet: $\Delta n_B = \pm .25g$

heavy buffet: $\Delta n_B = \pm .50g$

(U) These buffet boundaries are shown in Figure 3.3-31 as a function of Mach number. It is readily seen that the leading-edge flap design for Configuration 401B raises the buffet boundaries to a highly desirable level for buffet-free sustained turns at Mach 0.8/30,000-ft altitude.

(U) Configuration planforms of the 401B and FX-132 type generate large amounts of vortex lift after the main wing has stalled, and the maximum C_L is limited only by tail power. The control limit C_L for Configuration 401B is shown as the upper boundary in Figure 3.3-31 (also see Section 3.4).

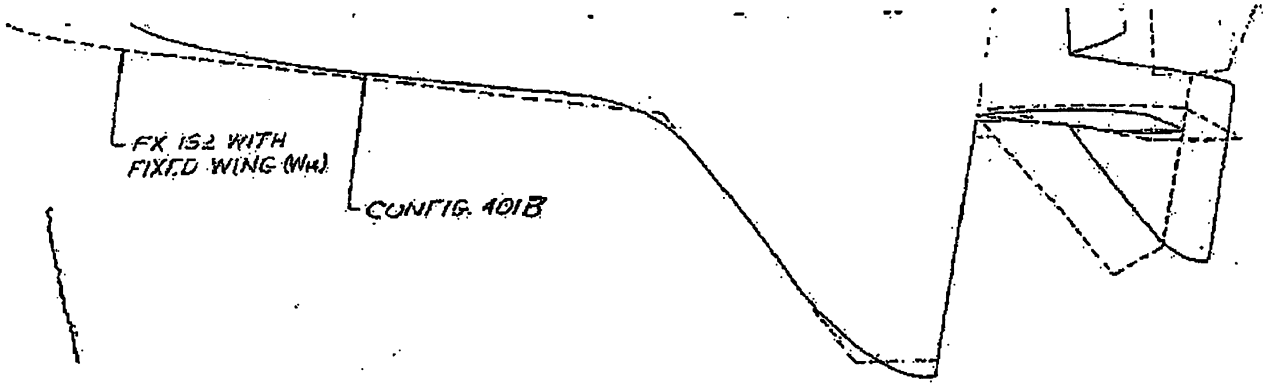

~~(S)~~ Figure 3.3-5 Planforms of Configuration 401B and the FX-132 Wind Tunnel Model (U)

(S) Figure 3.3-6 Drag Due to Lift at M=0.6, Configuration 401B (U)

(U) Figure 3.3-7 Drag Due to Lift at M=0.8, Configuration 401B (U)

(S) Figure 3.3-8 Drag Due to Lift at M=0.9, Configuration 401B (U)

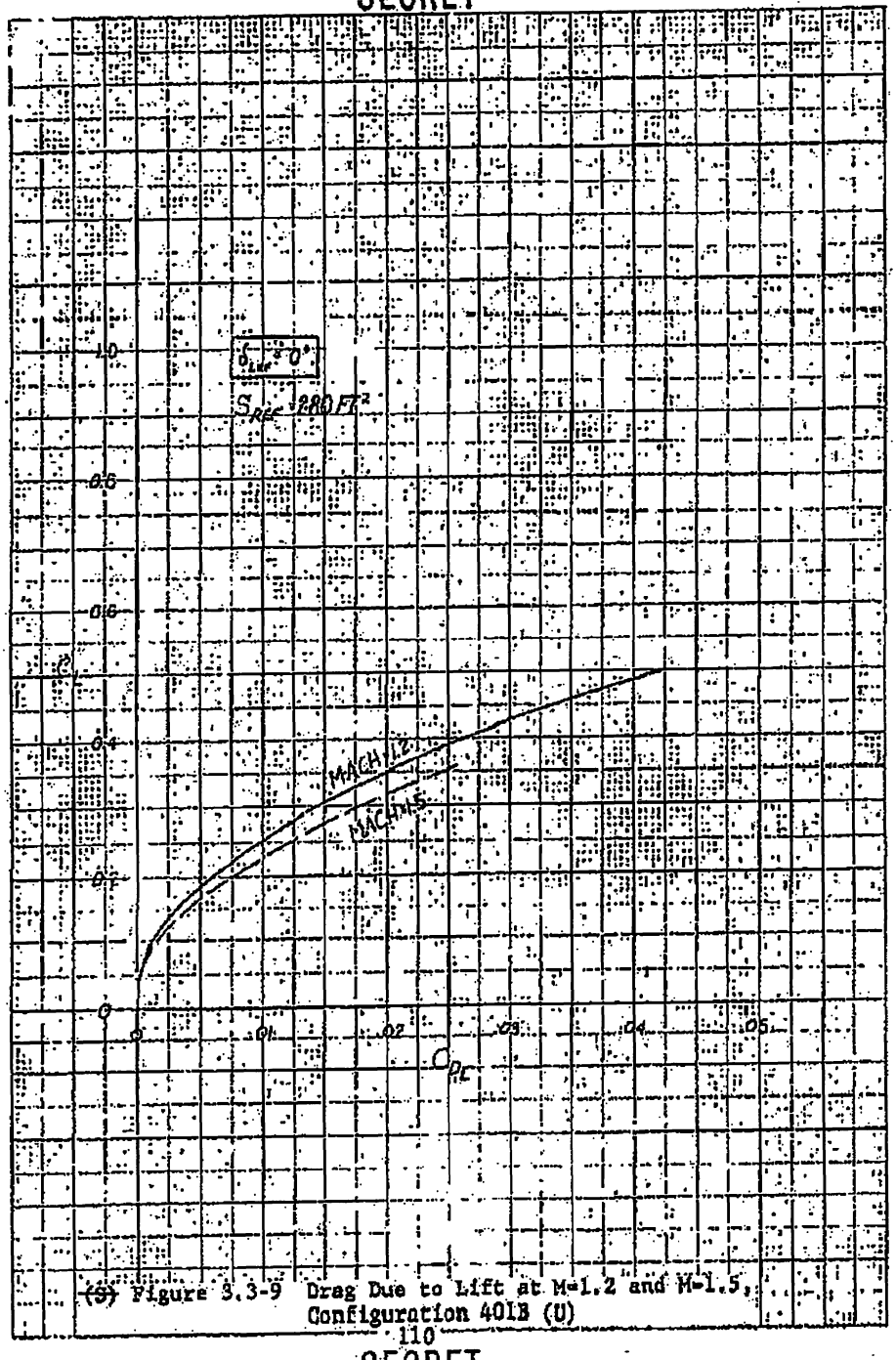

(S) Figure 3.3-9 Drag Due to Lift at M=1.2 and M=1.5, Configuration 401B (U)

(S) Figure 3.3-10 Drag Due to Lift at High C_L's, Configuration 401B (U)

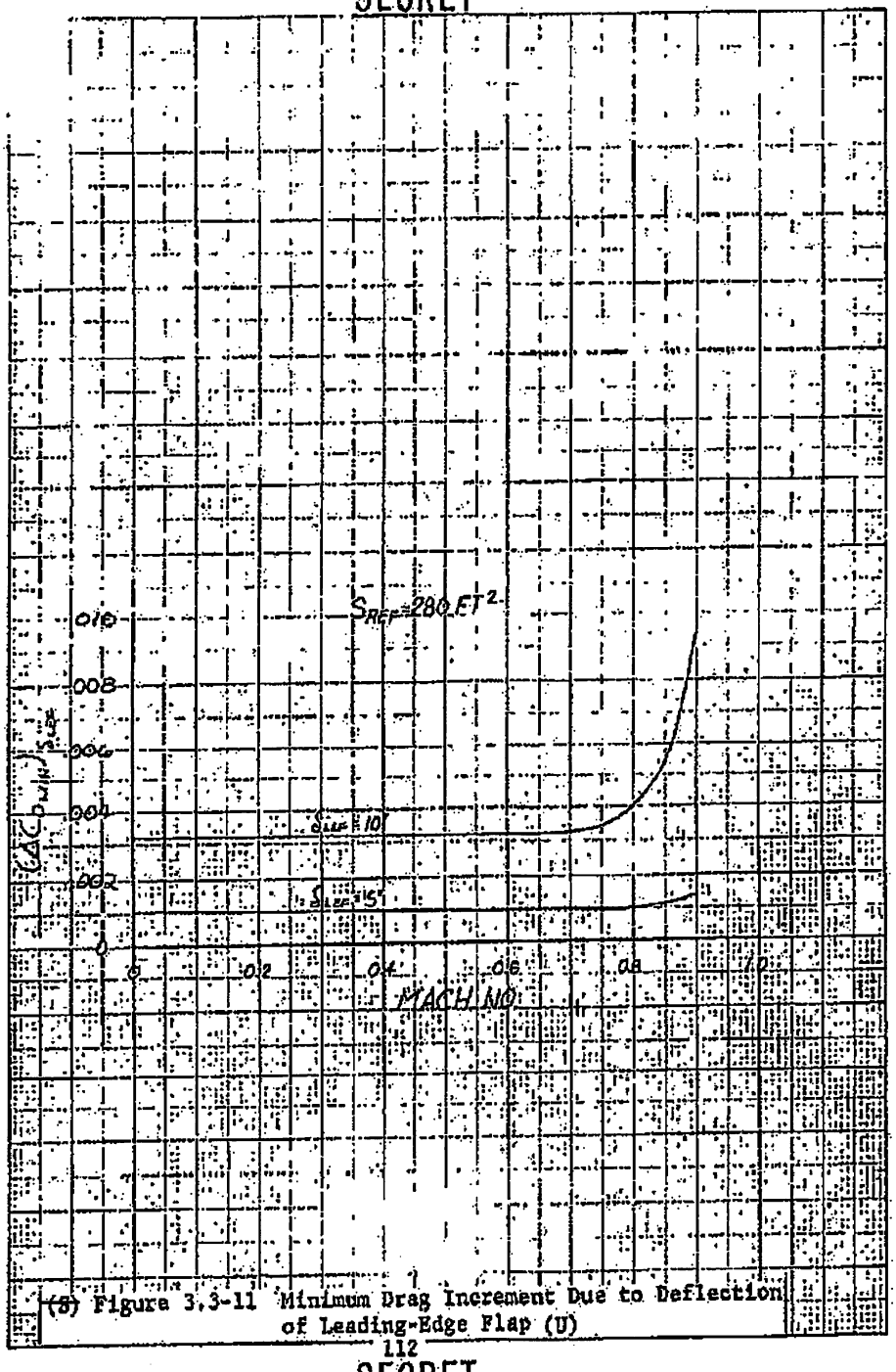

(S) Figure 3.3-11 Minimum Drag Increment Due to Deflection of Leading-Edge Flap (U)

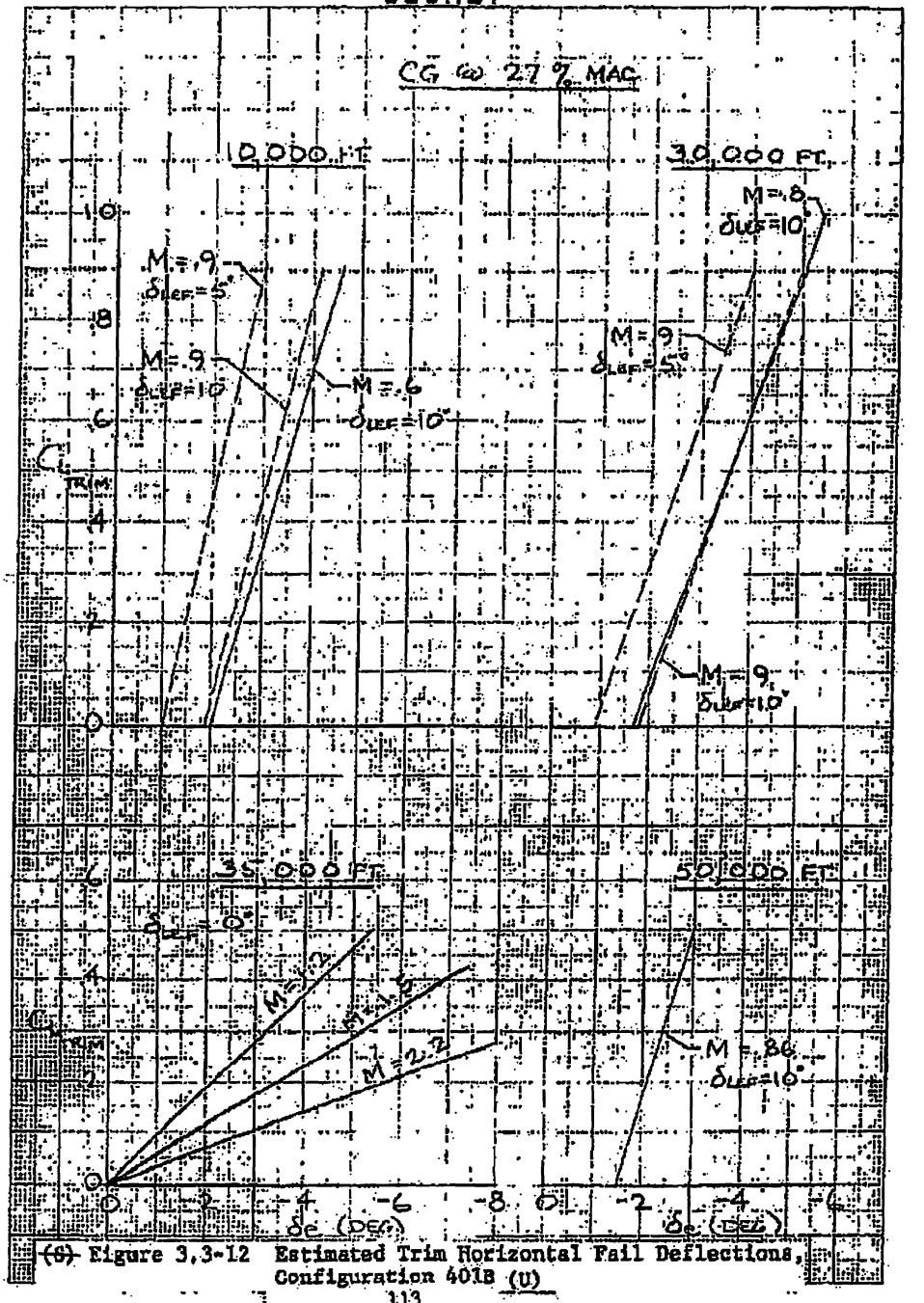

(S) Figure 3.3-12 Estimated Trim Horizontal Tail Deflections, Configuration 401B (U)

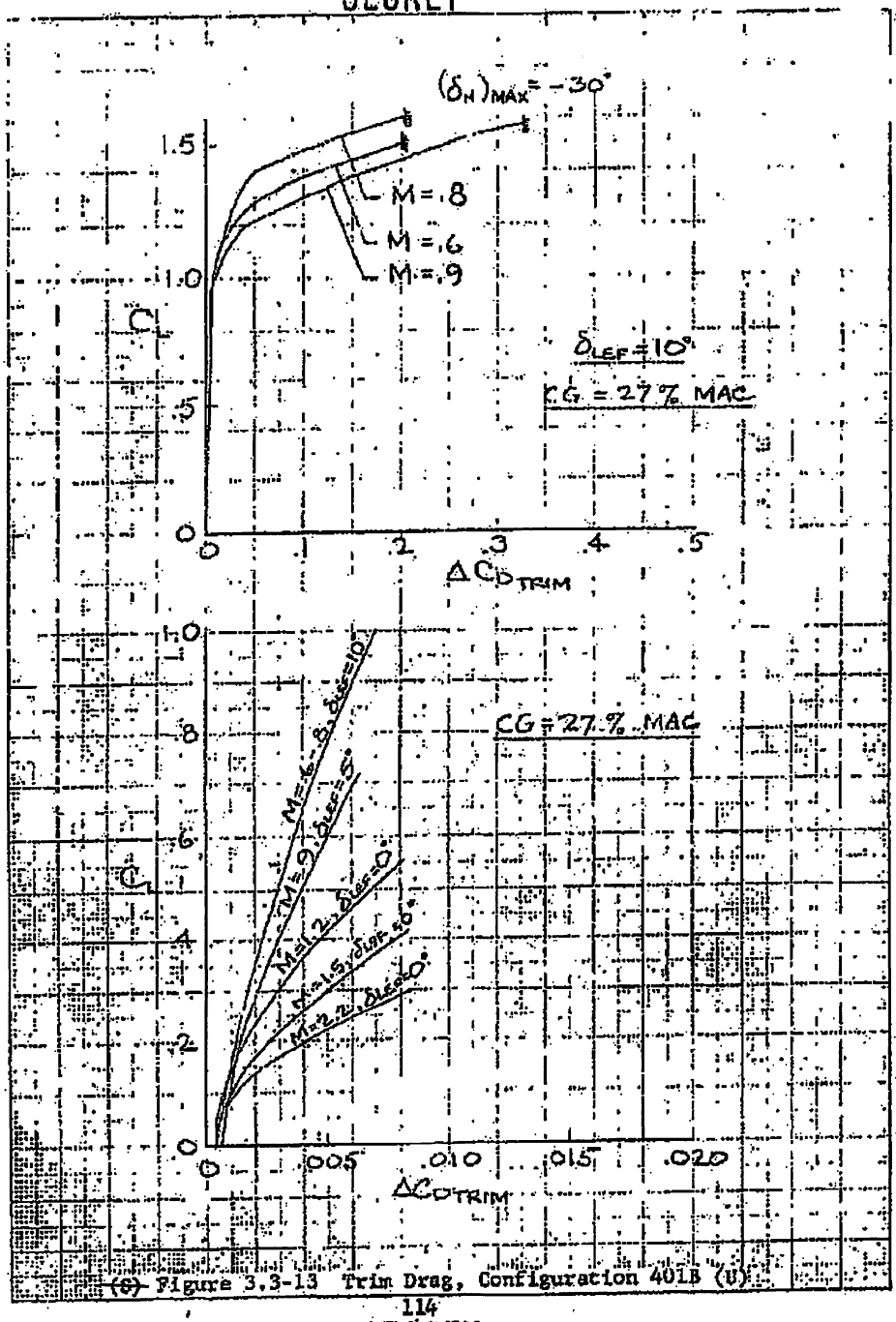

(S) Figure 3.3-13 Trim Drag, Configuration 401B (U)

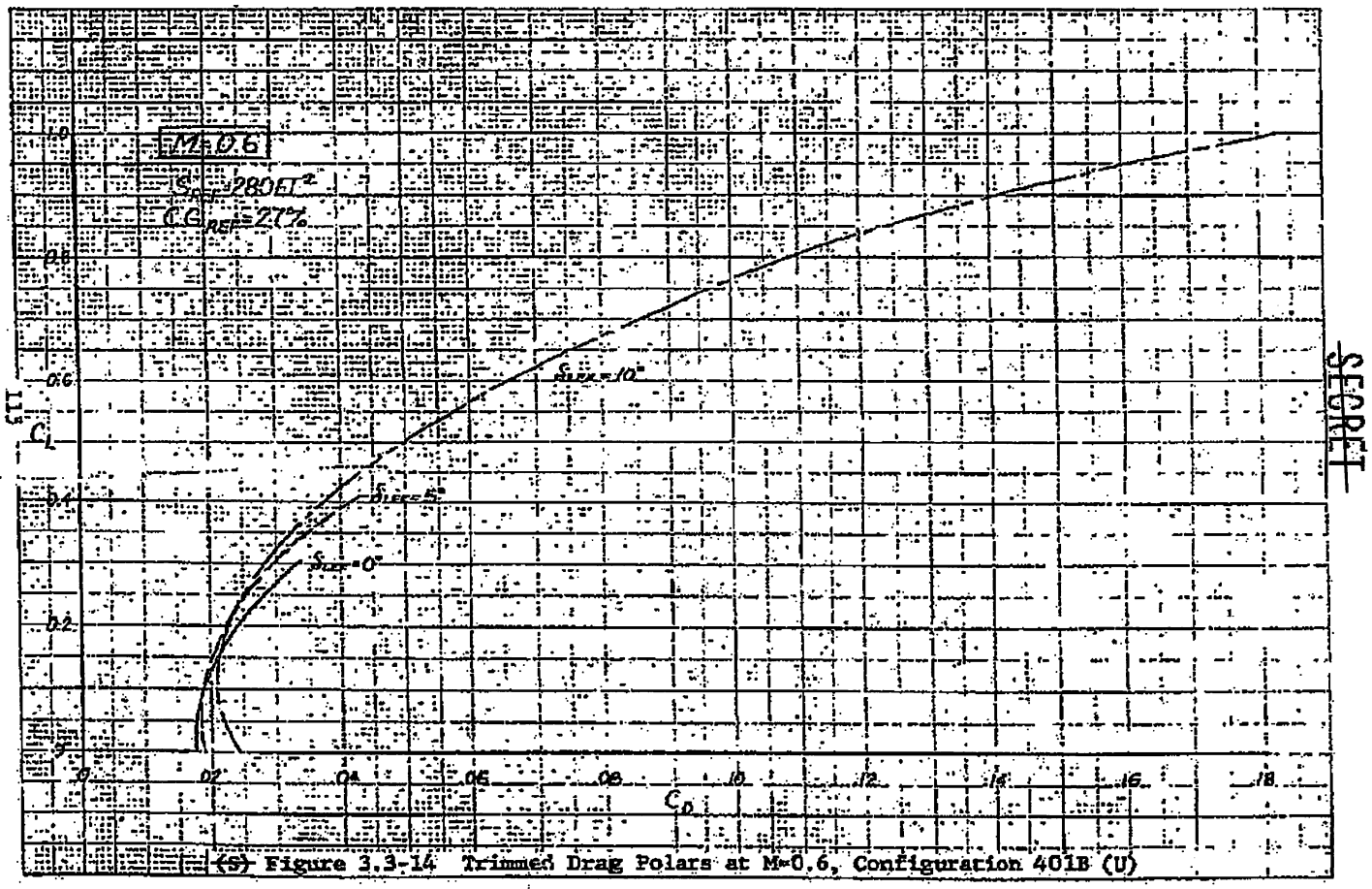

(S) Figure 3.3-14 Trimmed Drag Polars at M=0.6, Configuration 401B (U)

(S) Figure 3.3-15 Trimmed Drag Polars at M=0.8, Configuration 401B (U)

(S) Figure 3.3-16 Trimmed Drag Polars at M=0.9, Configuration 4018 (U)

SECRET

SECRET

117

88th ABW/IPI FOIA (b) (1) E.O.1352 6 SEC. 3.3(b)(4) 1.4(a)(g)

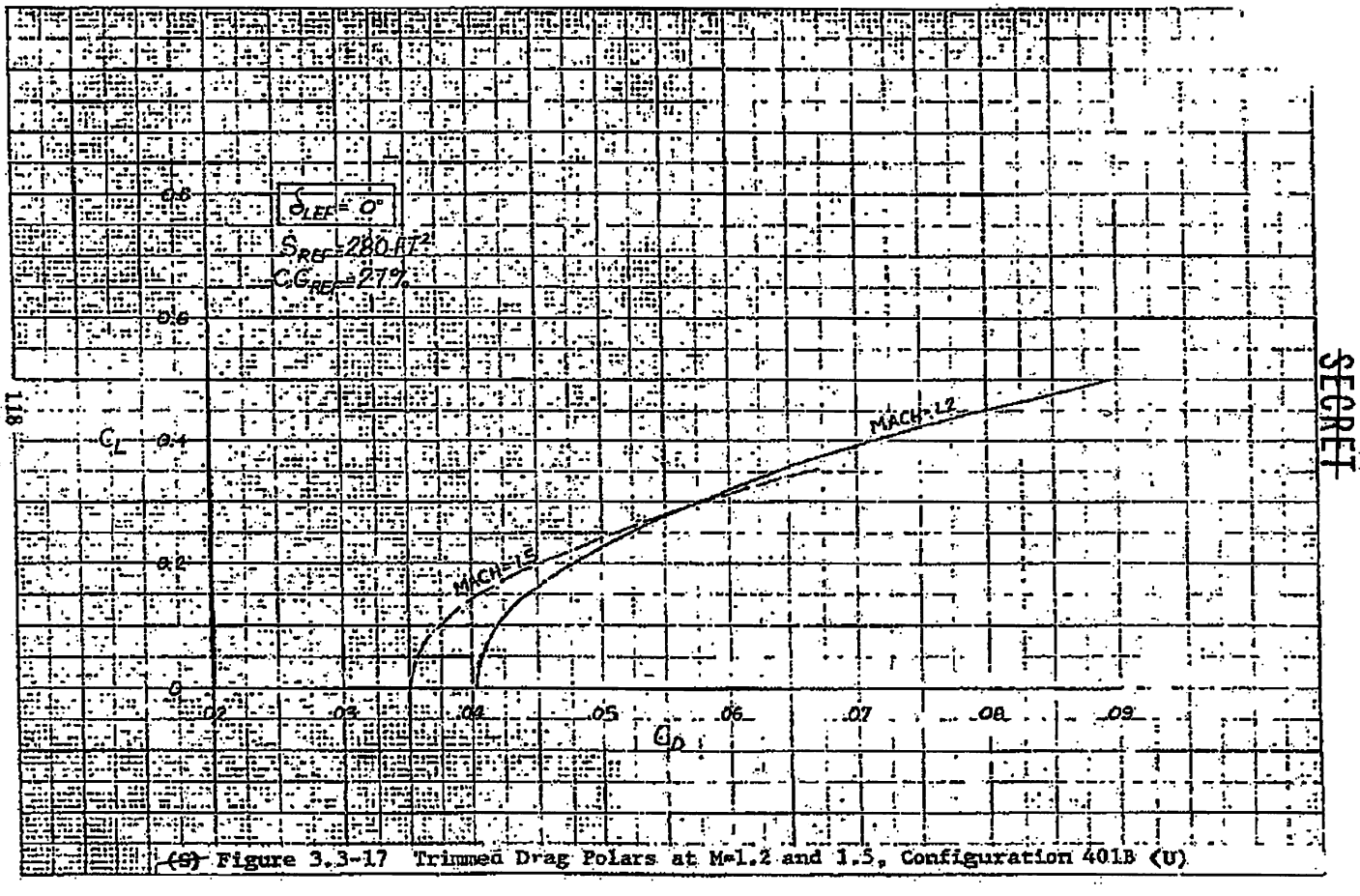

(S) Figure 3.3-17 Trimmed Drag Polars at M=1.2 and 1.5, Configuration 401B (U)

(S) Figure 3.3-18 Trimmed Drag Polars at High C_T's, Configuration 401B (U)

(S) Figure 3.3-19 Trimmed Takeoff and Landing Drag Polars, Configuration 401B (U)

(S) Figure 3.3-20 Trimmed Configuration Polars at M=0.6, Configuration 401B (U)

(S) Figure 3.3-21 Trimmed Configuration Polars at M=0.8, Configuration 401B (U)

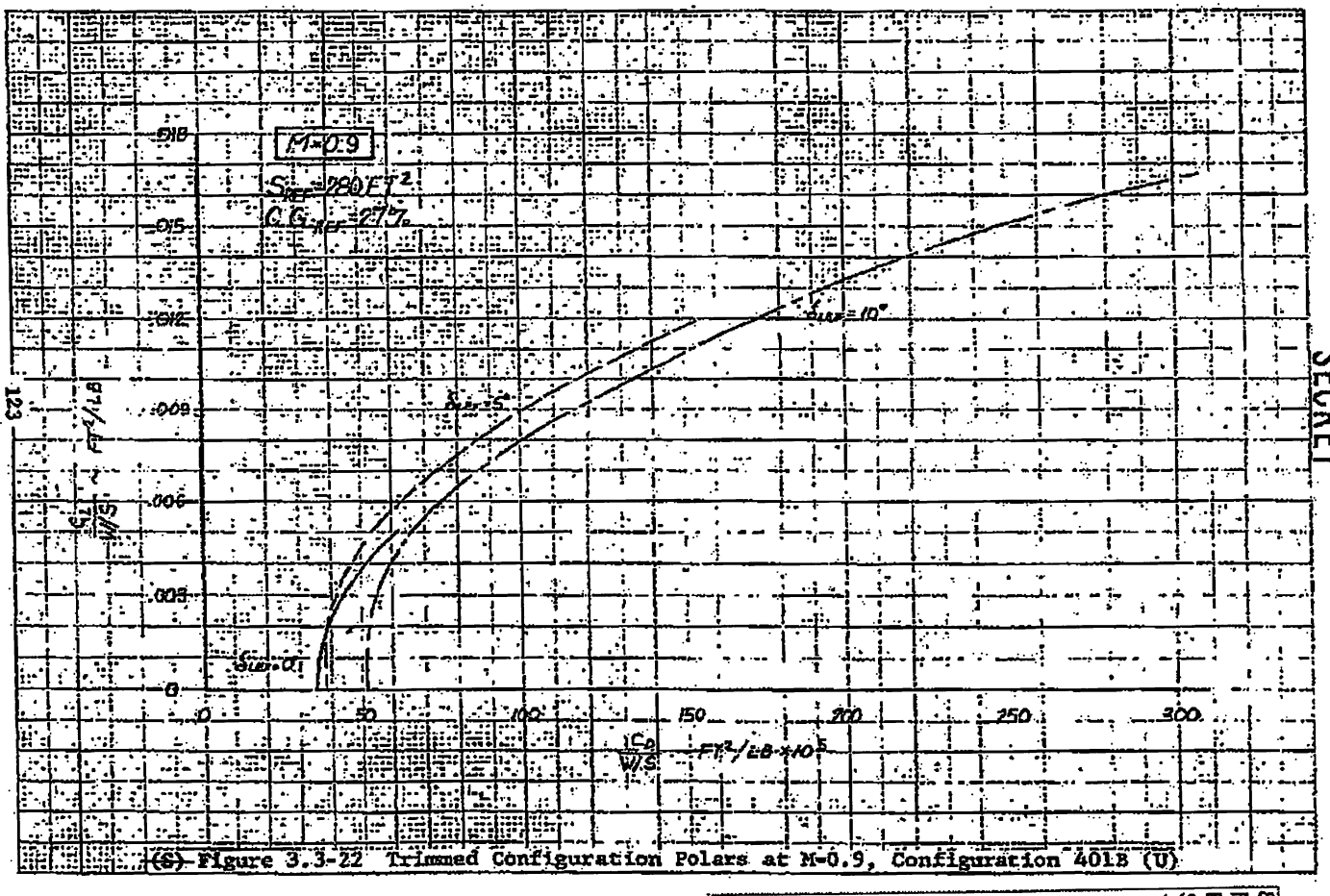

(S) Figure 3.3-22 Trimmed Configuration Polars at M-0.9, Configuration 401B (U)

SECRET

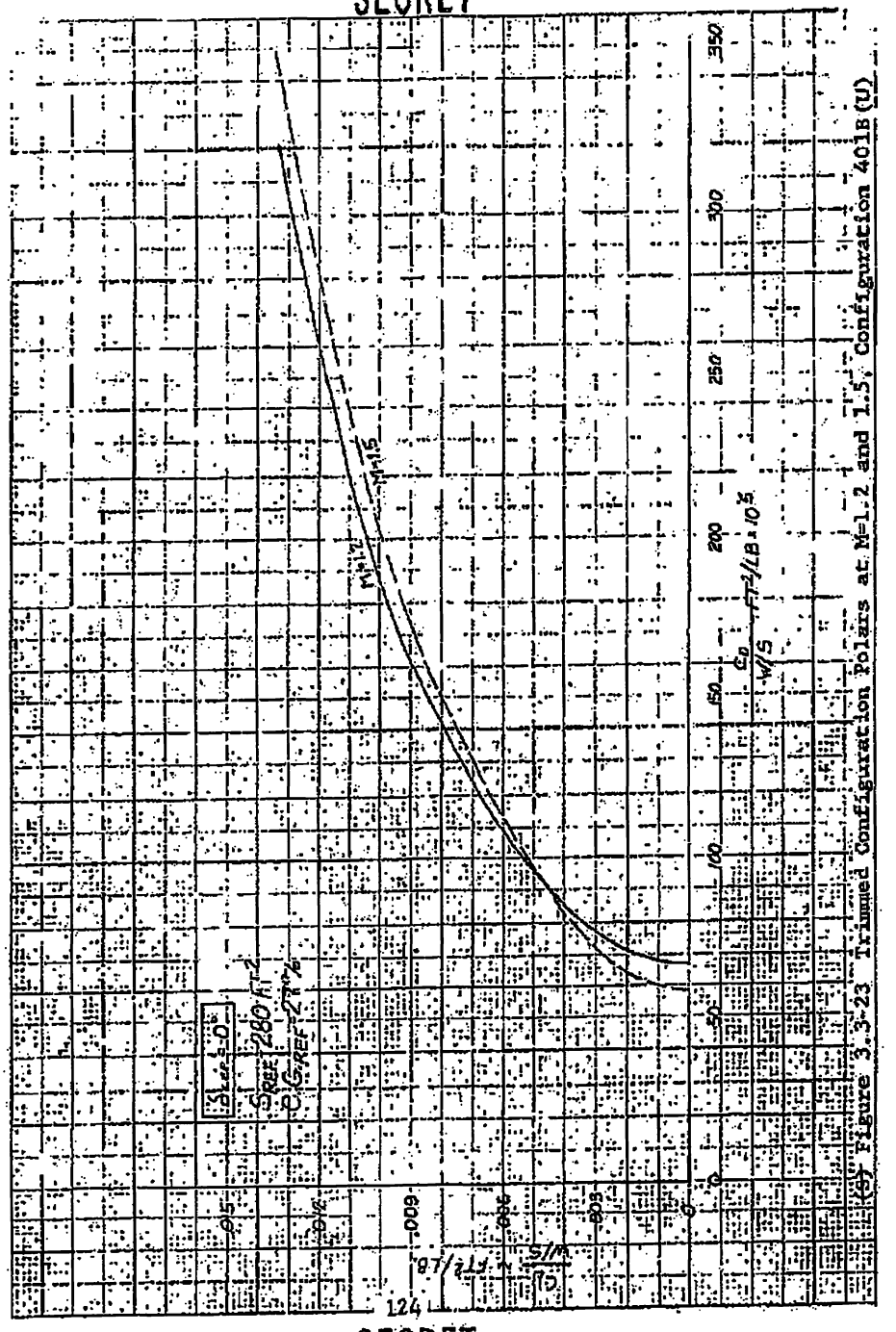

Figure 3.3-23 Trimmed Configuration Polars at M=1.2 and 1.5, Configuration 401B (U)

124

SECRET

88th ABW/IPI
FOIA (b)(1)
E.O.13526 SEC.
3.3.(b)(4)
1.4. (a)(g)

(S) Figure 3.3-24 Trimmed Configuration Polars at High C_L's, Configuration 401B (U)

(S) Figure 3.3-25 Trimmed (L/D) Max vs Mach Number, Configuration 401B (U)

SECRET

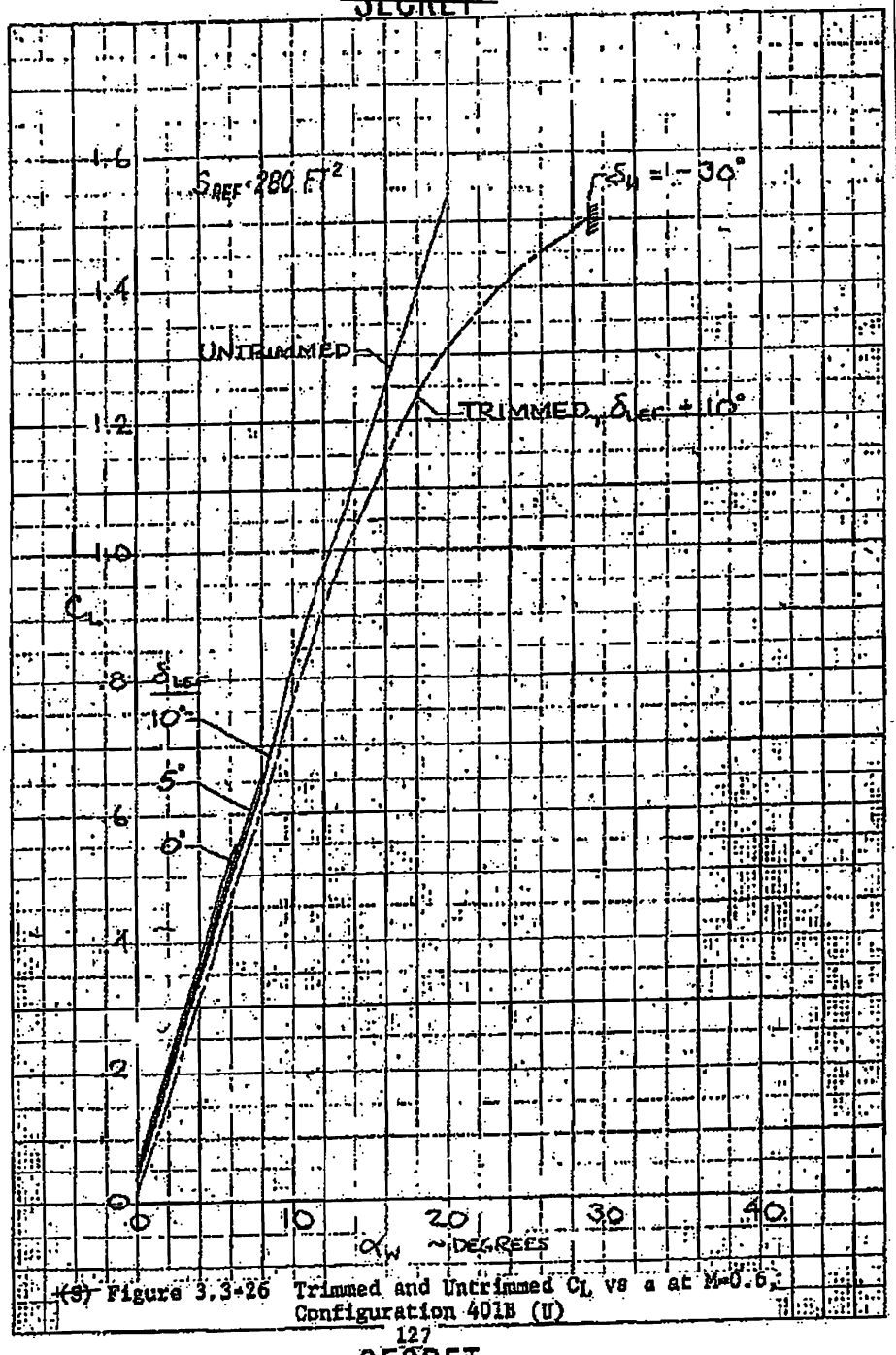

(S) Figure 3.3-26 Trimmed and Untrimmed C_L vs a at M=0.6, Configuration 401B (U)

SECRET

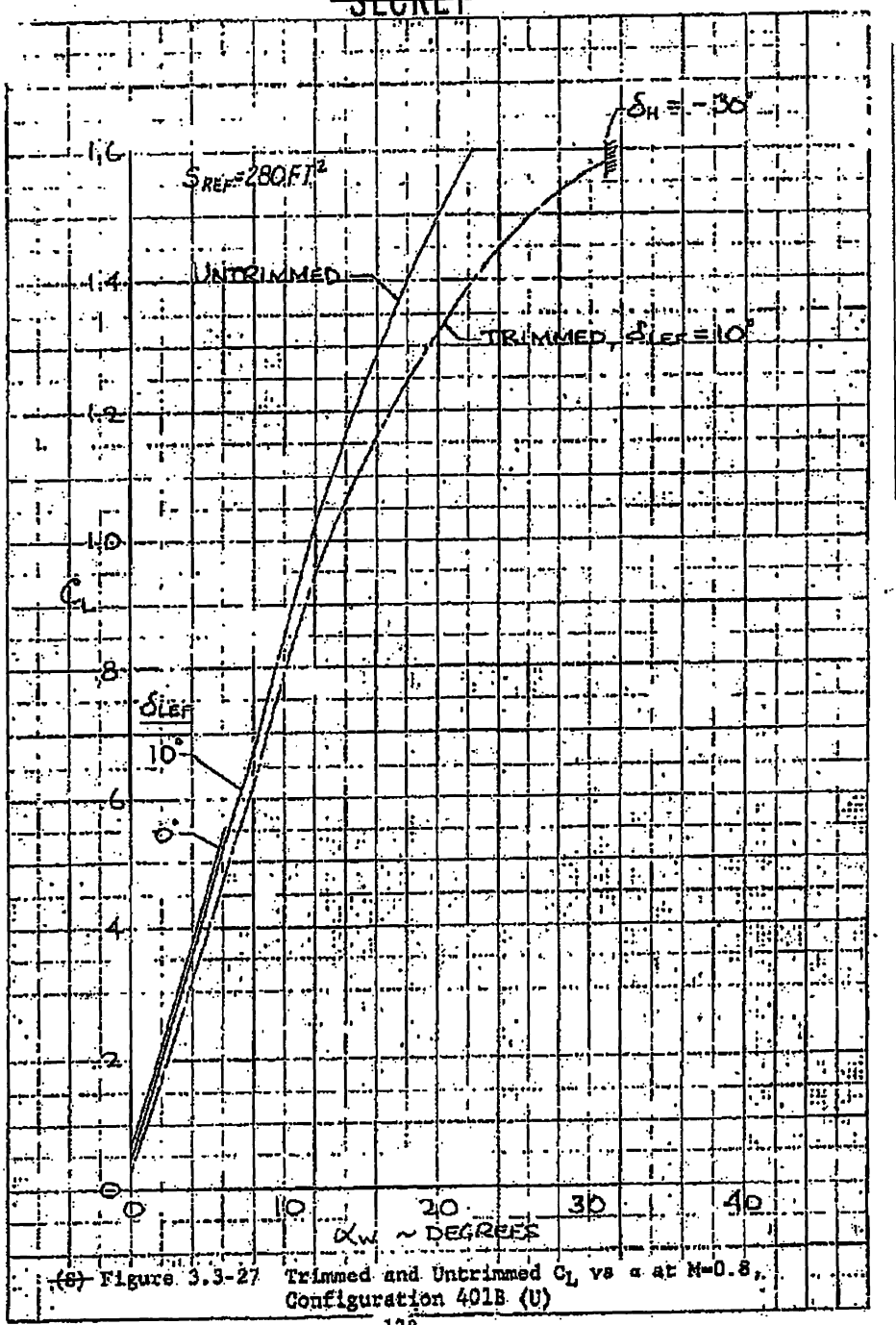

~~(S)~~ Figure 3.3-27 Trimmed and Untrimmed C_L vs α at M=0.8, Configuration 401B (U)

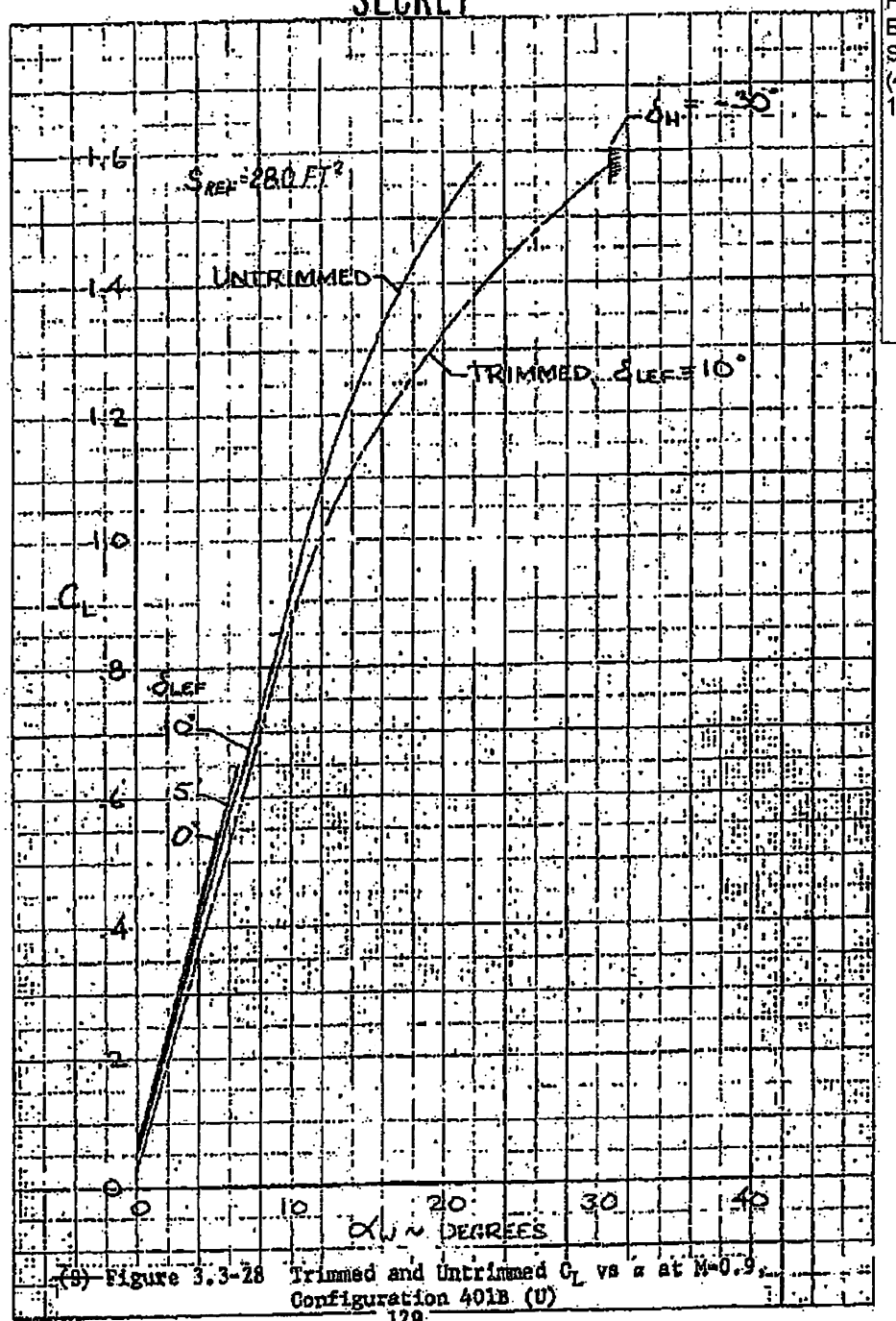

(S) Figure 3.3-28 Trimmed and Untrimmed C_L vs α at M=0.9, Configuration 401B (U)

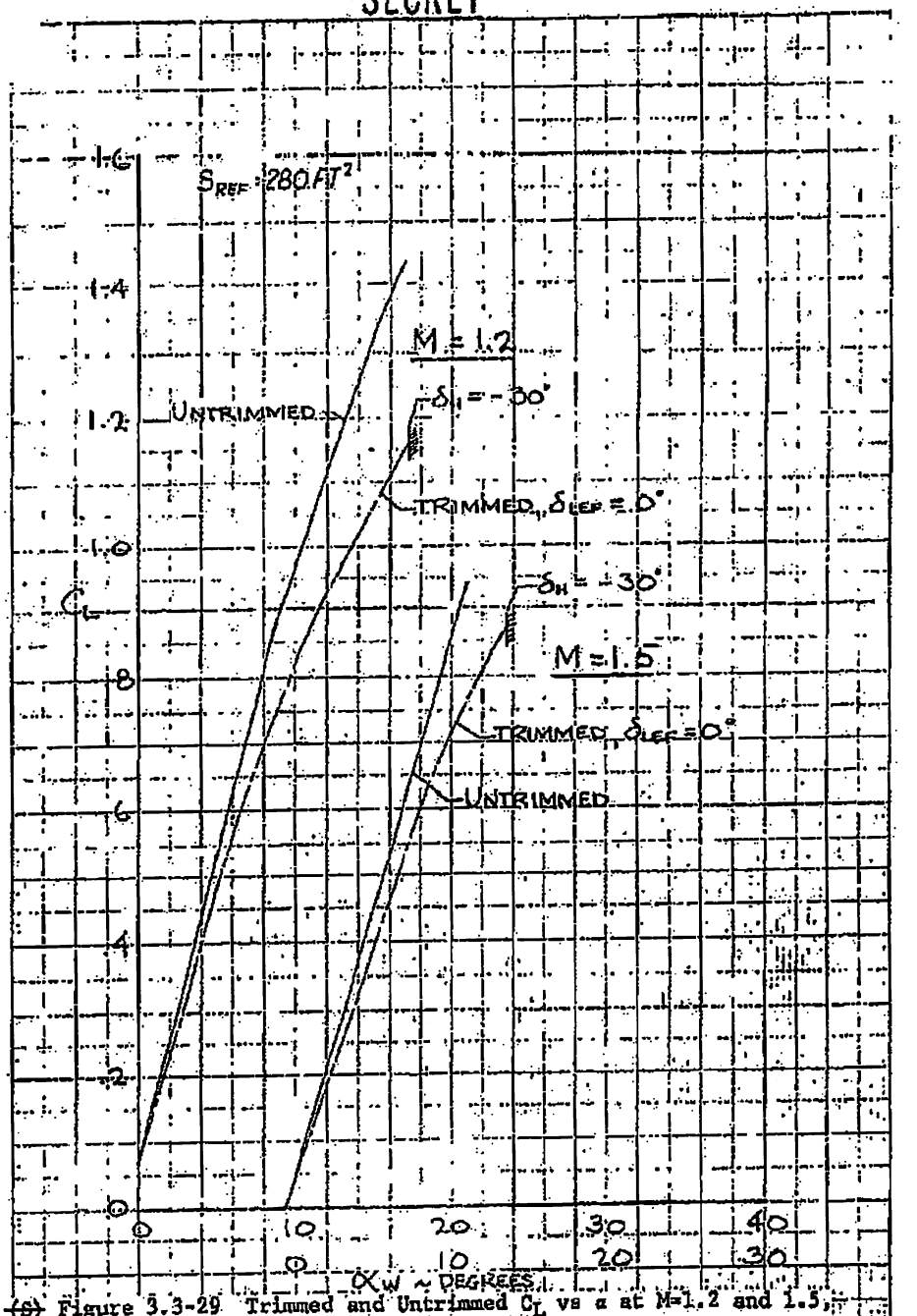

(S) Figure 3.3-29 Trimmed and Untrimmed C_L vs α at M=1.2 and 1.5, Configuration 401B (U)

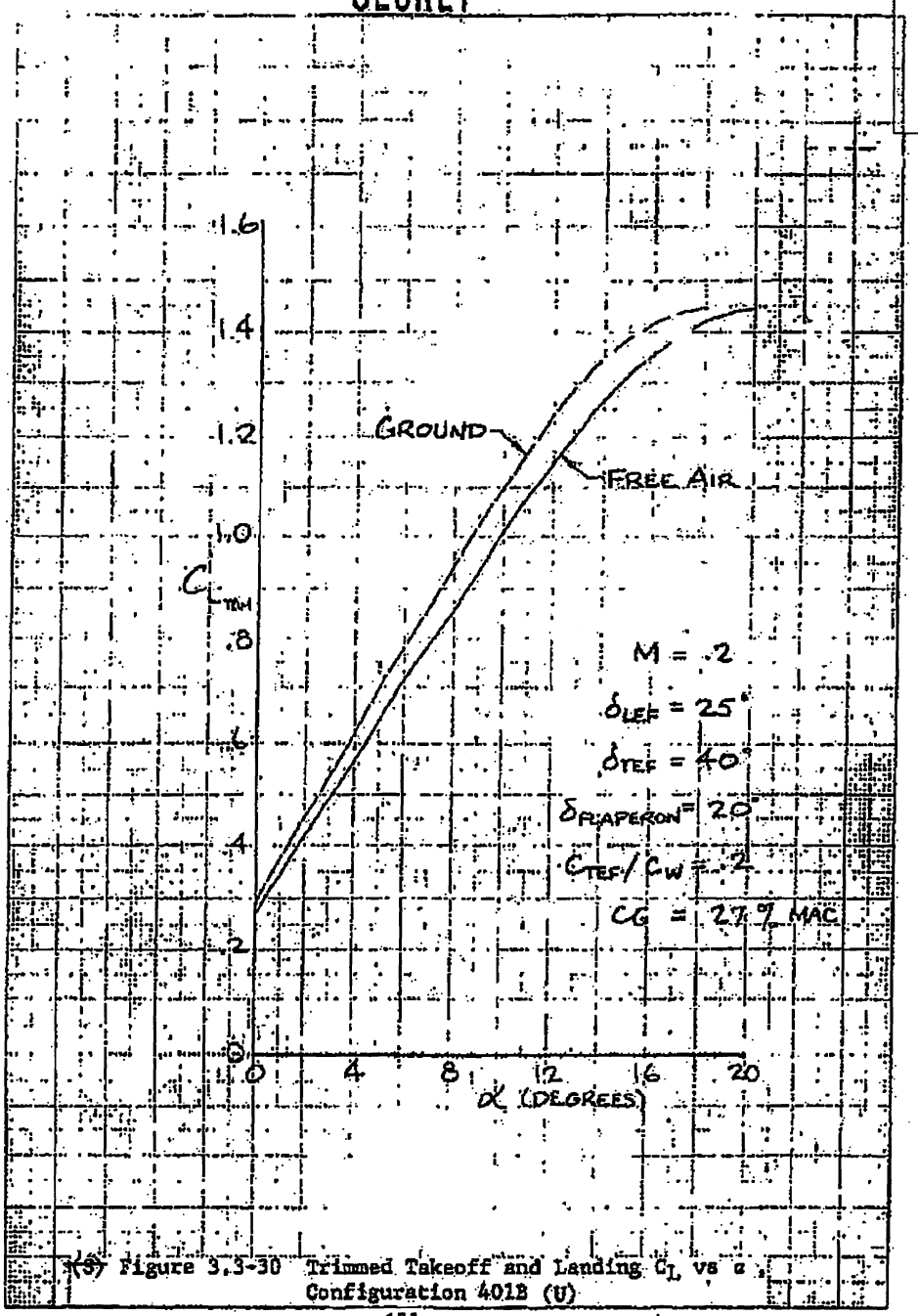

(S) Figure 3.3-30 Trimmed Takeoff and Landing C_L vs α, Configuration 401B (U)

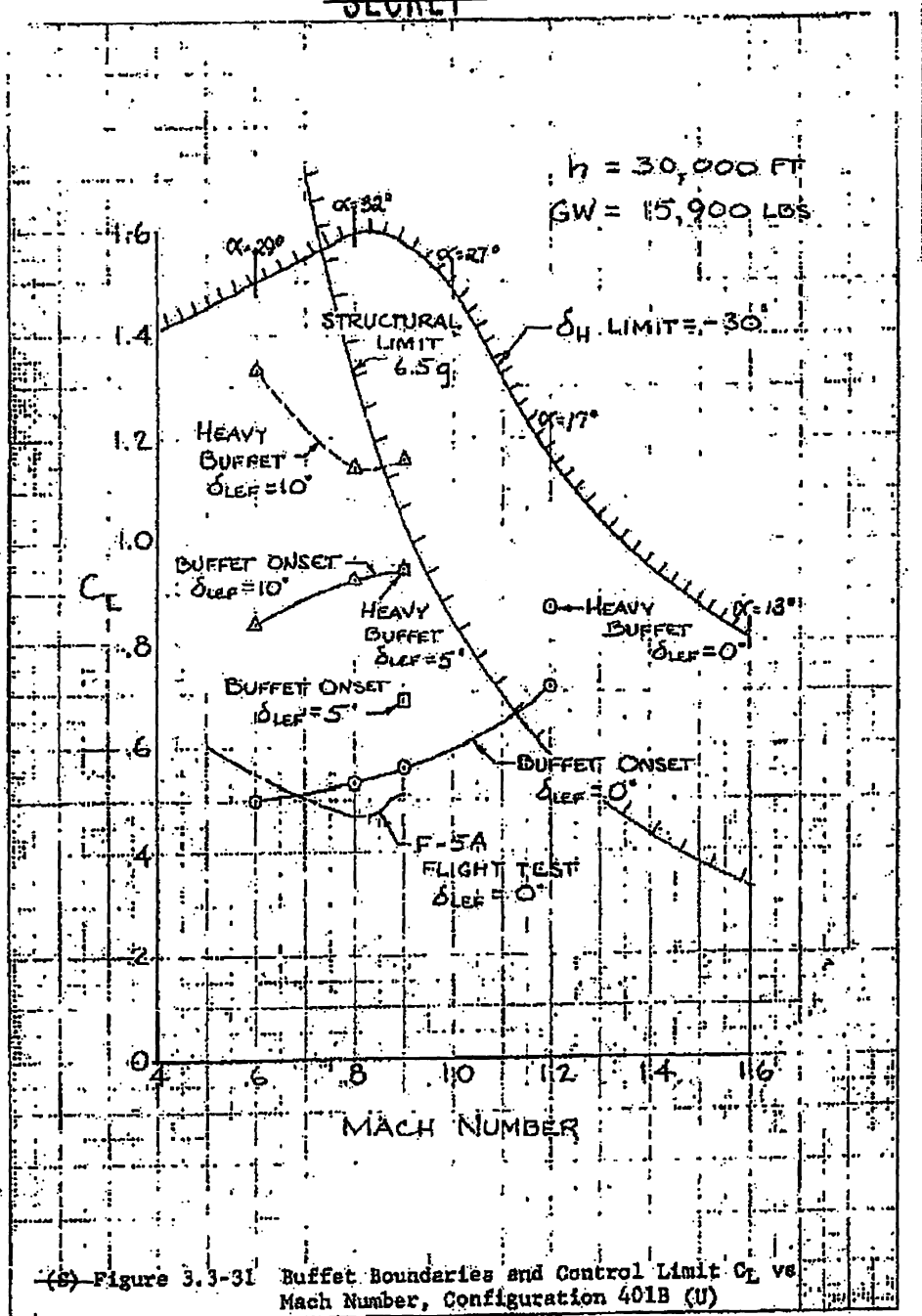

(S) Figure 3.3-31 Buffet Boundaries and Control Limit C_L vs Mach Number, Configuration 401B (U)

3.4 STABILITY, CONTROL, AND HANDLING QUALITIES

(U) Handling qualities/stability and control studies have been primarily directed toward identifying design features necessary to provide excellent handling qualities. This very demanding goal is basically achievable through proper aerodynamic configuration tailoring to ensure superior inherent longitudinal and lateral-directional stability and control. Pertinent results of the stability and control design techniques and the approach followed in support of this demanding goal of excellent fighter handling qualities are presented and discussed in this section.

3.4.1 Handling Qualities Design Rationale

(U) Specific stability and control design objectives that were followed in the development of Configuration 401B for excellent handling qualities in the combat region are listed in Table 3.4-1. The key factors in configuration design development are listed in the table for each of the objectives. Major benefits to be derived for each objective are also noted.

(U) In addition to the objectives listed in the table, low inertias are desirable for improved maneuver response with minimum-sized control and stabilizing surfaces.

3.4.2 Stability and Control Design Techniques

(U) General design guides to provide superior inherent stability and control characteristics were established. These design guides are related to pitchup, pitch control, directional stability, and aileron yaw and are discussed below in relation to wing planform, horizontal tail location, fuselage nose shape, vertical stabilizing surfaces, and aileron design.

(U) Wing Planform - Pitchup criteria from Reference 10 are presented in Figure 3.4-1. The wing planform pitchup boundary is given as a function of the wing aspect ratio and quarter chord sweep in the upper plot of Figure 3.4-1. Configuration 401B falls near the boundary in the satisfactory region. Proximity to the boundary in the satisfactory region is desirable in lieu of large displacement below the boundary. In general, the severity of the stable

(U) Table 3.4-1 HANDLING-QUALITIES DESIGN RATIONALE

OBJECTIVE	CONFIG. DESIGN APPROACH	BENEFITS DERIVED
NO PITCHUP	• WING GEOMETRY (AR vs. Λ RELATIONSHIP) • TAIL LOCATION (LOW)	• INCREASED COMBAT AGILITY • FULL MANEUVERING POTENTIAL AND PENETRATION INTO HEAVY BUFFET WITH NO PILOT FEAR OF NOSE UP TENDENCIES
NO AILERON YAW	• AILERON LOCATION (AIL./V.T. RELATIONSHIP FOR $C_{n_{\delta_a}} = 0$) • VERTICAL STABILIZING SURFACES (Hi V.T. Vol.)	• RAPID COORDINATED ROLL • PRECISE TRACKING • ANTI SPIN
NO WING ROCK	• WING PANEL GEOMETRY (CAMBER, TWIST, L.E. DEVICE) • WING PLANFORM (Hi $C_{L_{\alpha_W}}$ FOR INHERENT ROLL DAMPING)	• POSITIVE EFFECTIVE DIHEDRAL • STALLING OF LEADING WING PANEL DURING SIDESLIP AT HIGH ANGLES OF ATTACK ELIMINATED
NO DIRECTIONAL DIVERGENCE	• VERTICAL TAIL GEOMETRY AND LOCATION (Hi V.T. Vol., AR_{VT}, V.T./WING/BODY SIDEWASH RELATIONSHIP) • FUSELAGE FOREBODY CROSS SECTION • VENTRAL	• INCREASED COMBAT AGILITY AND MANEUVERABILITY • ANTI SPIN • POSITIVE DYNAMIC DIRECTIONAL STABILITY • NOSE SLICE ELIMINATED
CONTROL IN STALL	• TAIL LOCATION (BELOW WING CHORD PLANE IN LOW DOWNWASH REGION AND BELOW WING WAKE) • AILERON LOCATION (MID SPAN/OUTBOARD)	• POSITIVE CONTROL IN STALL • INCREASED COMBAT AGILITY • AIL./H.T. ROLL INTERFERENCE MINIMIZED • SPIN SUSCEPTIBILITY MINIMIZED
INHERENT DAMPING (FREE AIRFRAME)	• AERODYNAMIC STABILIZING SUR. (Hi TAIL Vol.) • WING PLANFORM (Hi $C_{L_{\alpha_W}}$)	• FAST SETTLING TIME • STABLE GUNNERY PLATFORM • PRECISE TRACKING CONTROL

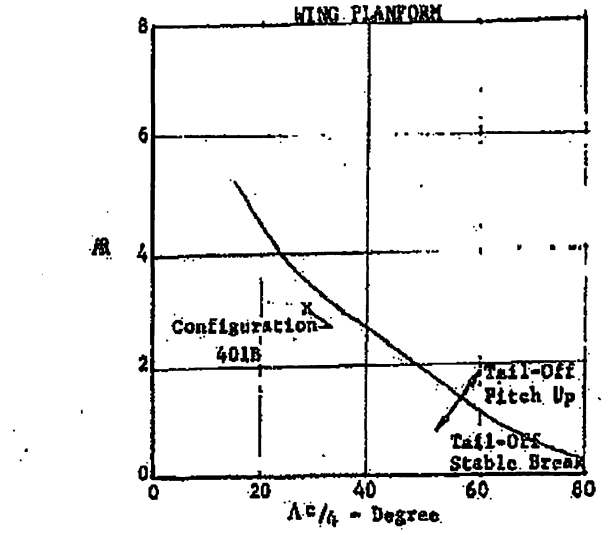

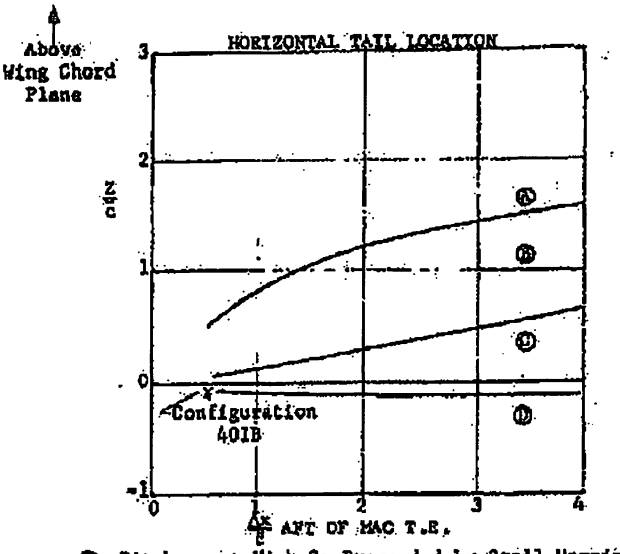

Ⓐ Pitch-up at High C_L Preceeded by Stall Warning
Ⓑ Pitch-up Without Warning
Ⓒ Generally No Pitch-up at Subcritical Speeds
Ⓓ Generally No Pitch-up

Reference: TM X-26

(U) Figure 3.4-1 NASA Pitch-up Criteria

break in the wing/body pitching moment is proportional to the displacement variation below the boundary. Severe stabilizing breaks have a detrimental effect in reducing the maneuvering control power, especially for a low horizontal tail location.

(U) Low Horizontal Tail - Horizontal tail placement of the 401B configuration falls in the low-tail region "D" in the lower plot of Figure 3.4-1. This low tail position, in combination with the good wing planform pitchup characteristics, assures near linear pitching moment characteristics at subsonic and transonic speeds. The horizontal tail below the wing chord plane is in the low downwash region to provide the desirable aft aerodynamic-center position at low subsonic speeds. The low tail remains in the low downwash region as the airplane rotates to high angles of attack and, thus, precludes its passing alternately from high to low downwash regions as it passes through the wing wake. The result is a desirable near linear pitching moment curve to high angles of attack. The horizontal tails mounted low and aft on the fuselage extensions also provide high trimming effectiveness. Another important aspect of the low tail is that it minimizes the transonic aft aerodynamic-center travel. The low horizontal tail is a key feature in configuration layout of an air superiority fighter.

(U) Fuselage Nose Ellipticity - Static directional stability is the most significant aerodynamic derivative affecting lateral-directional handling qualities. Maintaining a positive level of directional stability at very high angles of attack is a matter of major design importance. A contributing factor to the directional stability level is the instability of the fuselage. Proper tailoring of the fuselage nose forebody section can have a pronounced effect in reducing fuselage instability at high angles of attack (References 11 and 12). Fuselage forebody ellipticity with the major axis in the horizontal plane can greatly influence the overall improvement in fighter directional stability at high angles of attack, as represented in Figure 3.4-2. Forebody-shape ellipticity has been integrated into the 401B design.

(U) Model test data on the F-5 (Reference 13) and F-100 (Reference 14) airplanes substantiate the influence of an elliptical cross section shape on the fuselage nose toward improving the directional stability at high angles of attack. Tail-off directional stability derived from the F-5 is presented as a function of angle of attack in the upper plot of

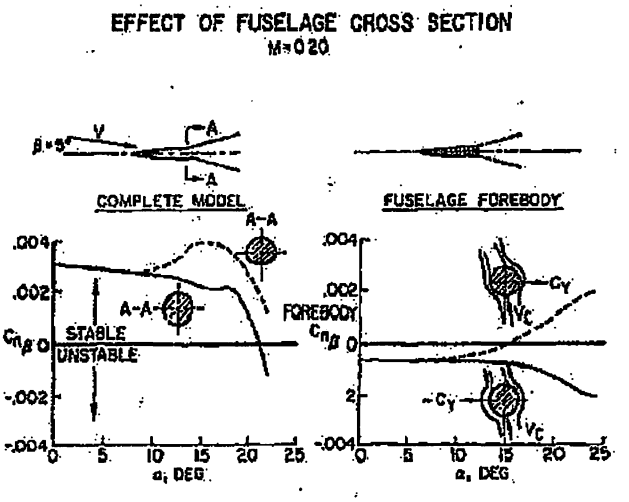

(U) Figure 3.4-2 Effect of Fuselage Forebody on Directional Stability

Figure 3.4.3. Above an angle of attack of about 16 degrees there is a decided improvement in stability with increasing angle of attack. This improvement is attributed to the F-5 nose ellipticity.

(U) Supersonic directional stability data at Mach 1.6 for the F-100 with the vertical tail off is also shown in this plot. At an angle of attack of approximately 16 degrees, there is a definite stabilizing trend in the high-angle-of attack range. Such improvement in stability level for the F-100 is also attributed to the fuselage nose ellipticity.

(U) Also in Figure 3.4-3 (lower plot), a comparison is given of the nose ellipticity of the 401B configuration with that of the F-5 and F-100. The nose ellipticity is shown as a function of percent fuselage length, and it is evident that all three have essentially the same level of ellipticity. Consequently, it is projected into the upper plot (dashed line) that Configuration 401B will possess the same favorable improvement in directional stability at high angles of attack.

(U) Twin Fins and Ventrals - Another important design aspect followed in providing good directional stability to high angles of attack is the location of the vertical stabilizing surfaces. The most important single parameter in defining tail effectiveness at high angles of attack is the amount of vertical surface area above and clear of destabilizing vortices generated by the fuselage nose, the canopy, and the wing/body intersection. On the basis of these considerations, outboard twin fins on aft fuselage extensions with ventrals projecting directly below and in the plane of upper fins have been selected to serve as effective stabilizing surfaces to very high angles of attack.

(U) Mid-Outboard Ailerons - Configuration factors which influence aileron yaw have been investigated for preliminary design guidelines. It has been found that aileron deflection produces yawing moment primarily by two effects, namely, side forces induced on the vertical tail/aft fuselage and differences in drag increments for the up-going and down-going controls. For the case of an air superiority fighter, major factors in order of importance are:

1. Vertical tail location with respect to ailerons
2. Wing height on the fuselage

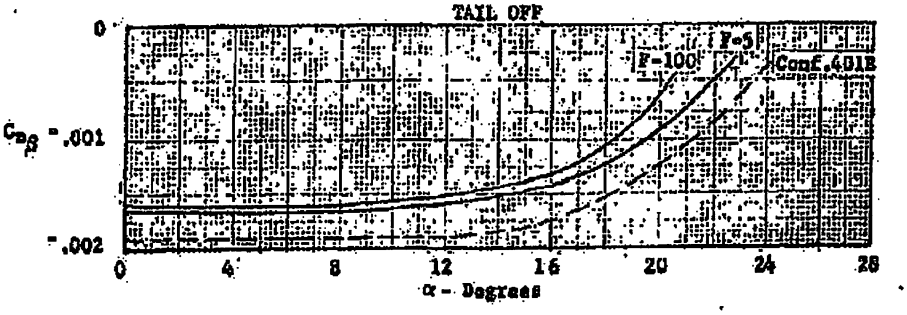

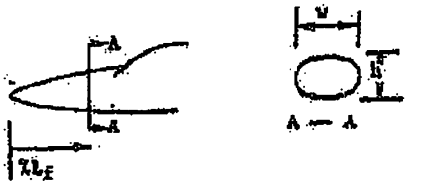

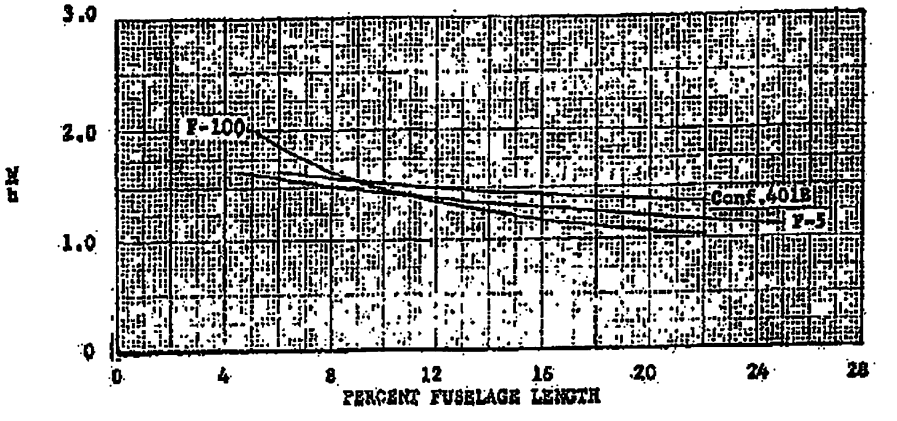

(U) Figure 3.4-3 Fuselage Nose Ellipticity

3. Drag differential of the up-going versus the down-going controls.

Factors 1 and 2 are basically related to the increased pressure field induced above the up-deflected surface, and are particularly potent at transonic and supersonic speeds because of the presence of strong shock waves. Generally, vertical tail location determines the level of yawing moment due to aileron. Drag variations with control deflection are the chief source of adverse yaw. Factor 3 would be dominant only for high-aspect-ratio wings with outboard ailerons. In fact, each of the factors is influenced by wing planform and section geometry, with sweep angle being of particular importance to Factors 1 and 2.

(U) On the basis of the aileron yaw investigation results, a configuration design guideline providing desirable vertical tail locations based on aileron yaw characteristics has been developed and is presented in Figure 3.4-4. Vertical tail location relative to the aileron is specified in terms of profile angle in the vertical plane and planview angle in the horizontal plane. The desirable region of vertical tail location indicated in Figure 3.4-4 is based upon transonic aileron-control yawing-moment data for the number of specific configurations listed. Configurations with large planview angles tend to have strong adverse yaw and thus would be susceptible to aileron-induced spins. Configurations with extremely low planview angles should also be avoided, since excessive proverse yaw is a prime contributor to lateral-directional pilot-induced oscillations. In general, the latter configurations would normally have inboard ailerons in close proximity to the horizontal tail. Such an arrangement may have large roll-control power losses due to horizontal tail interference effects. It is seen that the Configuration 401B aileron/vertical tail arrangement is in the acceptable region.

(U) A low wing height position on the fuselage also contributes to proverse aileron yaw due to induced aileron sidewash on the aft body. The opposite effect, or adverse yaw occurs with a high wing on the body. For a mid-wing on the body such as configuration 401B, a neutral effect from the body contribution due to aileron sidewash is experienced.

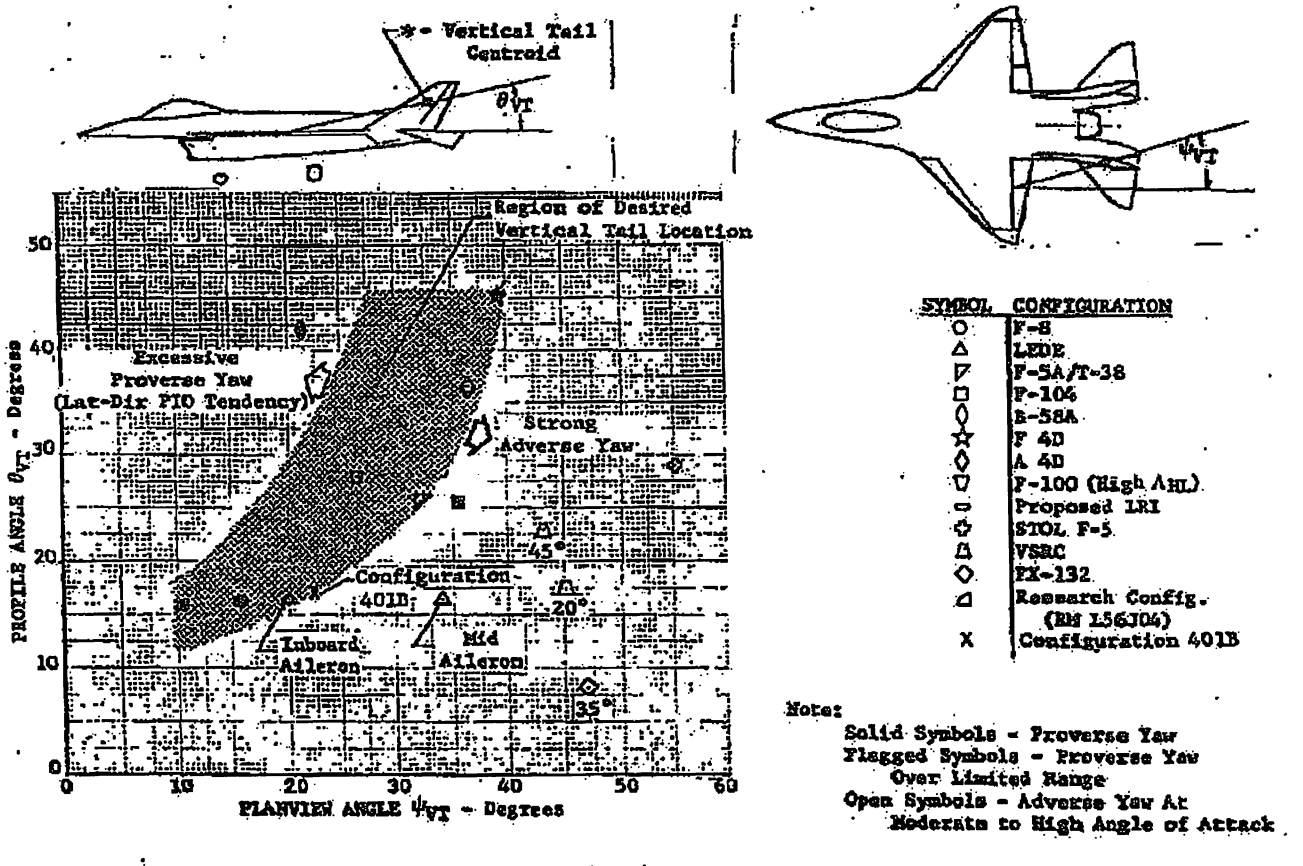

(U) Figure 3.4-4 Desirable Vertical Tail Locations Based on Aileron Yaw Characteristics

3.4.3 Stability and Control Basic Data

(U) Stability and control characteristics are the fundamental contribution to handling qualities. In this subsection, the predicted basic stability and control derivatives used in developing the predicted handling qualities of the 401B configuration are presented. In general, standard NASA symbols and definitions are employed, with the forces referred to the wind axes and the moments referred to the stability axes except in the cases for the dynamic directional stability and lateral control spin parameters, which are referred to the body axes system.

3.4.3.1 Longitudinal Stability and Control

(U) The two prime basic stability characteristics, namely, aerodynamic center and elevator control effectiveness are presented as functions of Mach number in Figures 3.4-5 and 3.4-6. Straight-forward analytical techniques, successfully used and proven reliable in the past for similar wing planform configurations and tails, have been employed to develop these characteristics. The effects of aeroelasticity, based on fixed-wing FX estimates, have been included.

(U) Weight and balance characteristics of Configuration 401B are listed in Table 3.4-2.

~~(S)~~ Table 3.4-2 WEIGHT & BALANCE CHARACTERISTICS

Gross Weight (lb)	C.G. (% MAC)
16,800 (full up)	24.9
12,614 (zero fuel)	21.2
11,981 (basic operating weight)	22.4
11,582 (weight empty)	24.7

With a low-speed aerodynamic center of 30% MAC, adequate static margin is provided for the takeoff and landing conditions. Similarly, positive static margins are available throughout the flight envelope. A detail summary of weight and balance is presented in Section 3.5.

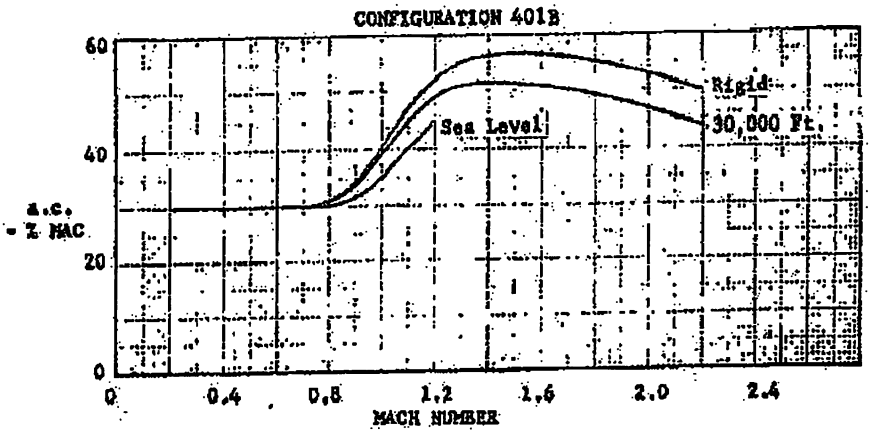

(U) Figure 3.4-5 Aerodynamic Center vs Mach Number

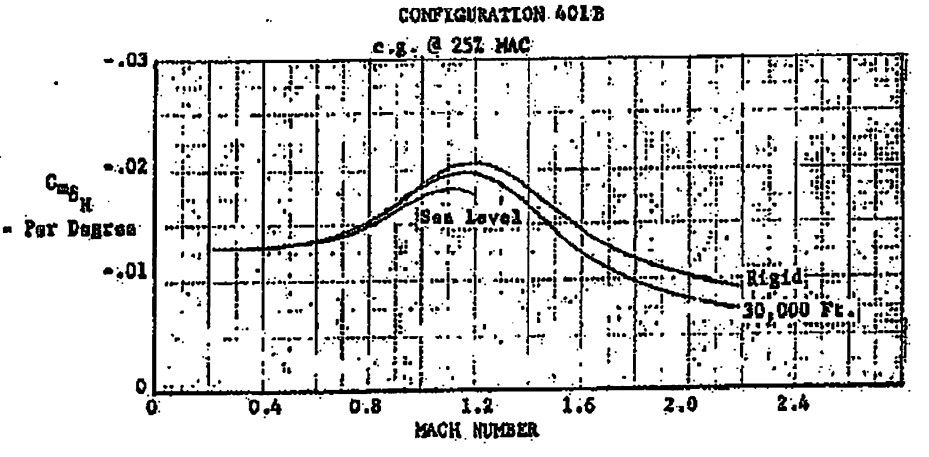

(U) Figure 3.4-6 Elevator Control Effectiveness vs Mach Number

(U) Estimated pitch damping is presented as a function of Mach number in Figure 3.4-7 and a function of angle of attack in Figure 3.4-8. Pitch dynamic-model test data (see Paper 4 of Reference 11) substantiates that the blended wing/body of Configuration 401B will maintain a good positive level of pitch damping at high angles of attack near the stall.

3.4.3.2 Lateral-Directional Stability and Control

(U) Static directional stability is the most significant stability derivative that affects lateral-directional handling qualities. Predicted directional stability of the twin-fin/ventral arrangement is shown for zero angle of attack as a function of Mach number in Figure 3.4-9 and for a Mach number of 0.8 as a function of angle of attack in Figure 3.4-10. Standard prediction techniques for vertical tail effectiveness were employed. The variation in vertical tail stabilizing effectiveness with angle of attack has been patterned after the FX twin-fin model data. Vertical tail aeroelastic effects shown are based upon FX estimates. The effectiveness of the ventrals in providing directional stability was derived through proper ventral volume coefficient corrections applied to FX model ventral test data. Body instability at low angles of attack was estimated according to Multhopp's method.

(U) The high levels of directional stability indicate good lateral-directional handling qualities to angles of attack well above limit buffet and well past maneuver limit, as shown in Figure 3.4-10. The improvement in directional stability at the very high angles of attack in Figure 3.4-10 is attributed to the forebody nose ellipticity, as described in Subsection 3.4.2. This favorable forebody contribution to improve body instability at high angles of attack is based on F-5 and F-100 body directional stability data as shown in Figure 3.4-3.

(U) Static lateral stability in terms of effective dihedral is presented as a function of Mach number in Figure 3.4-11 and as a function of angle of attack in Figure 3.4-12. The predicted variations are patterned after similar data for the F-5 airplane. Positive dihedral effect is apparent even to high angles of attack. The positive level of effective dihedral shown at high angles of attack precludes the presence of wing rock.

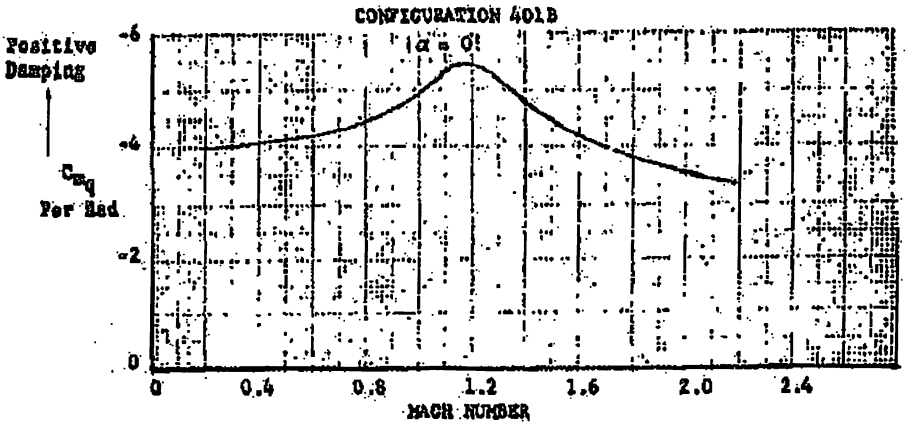

(U) Figure 3.4-7 Pitch-Rate Damping vs Mach

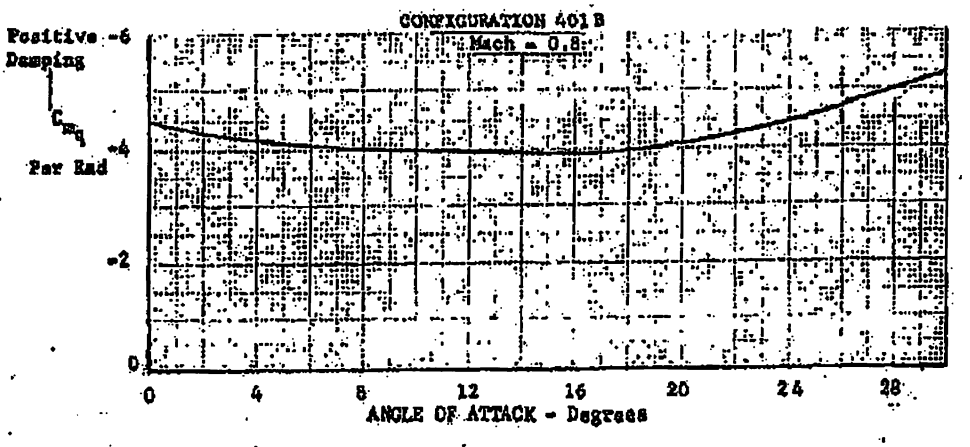

(U) Figure 3.4-8 Pitch-Rate Damping vs Angle of Attack

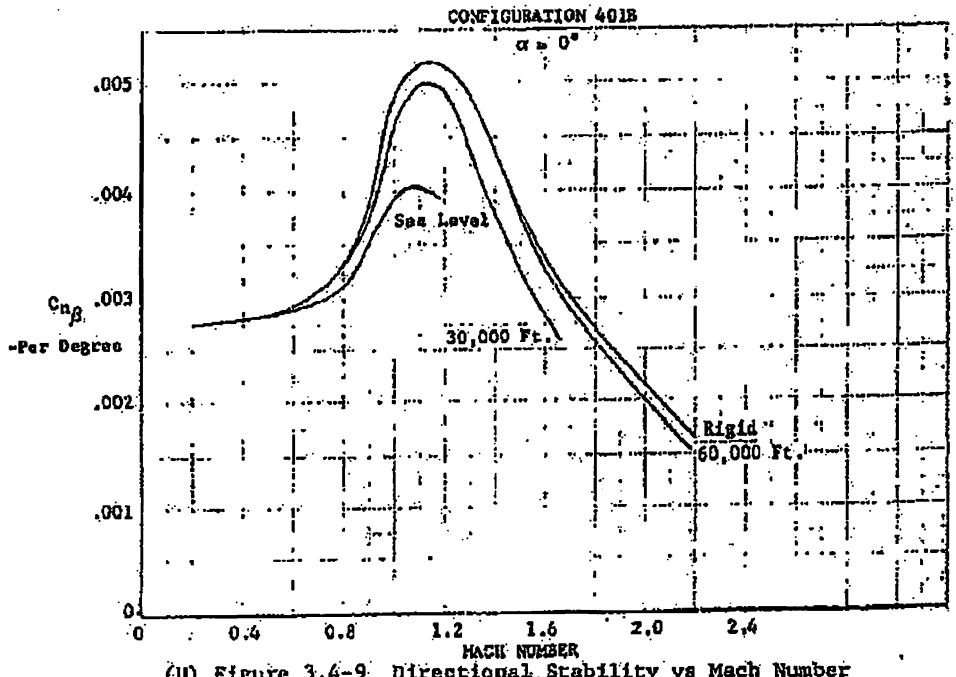

(U) Figure 3.4-9 Directional Stability vs Mach Number

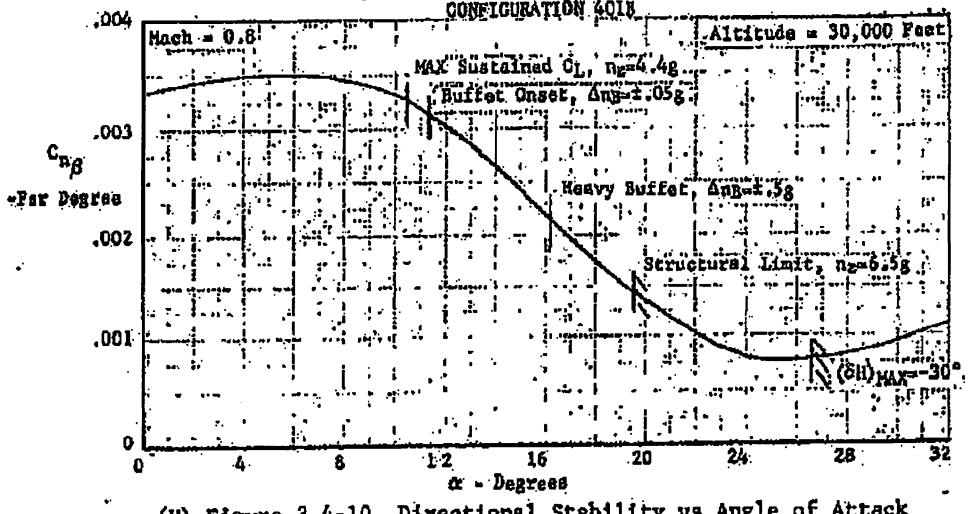

(U) Figure 3.4-10 Directional Stability vs Angle of Attack

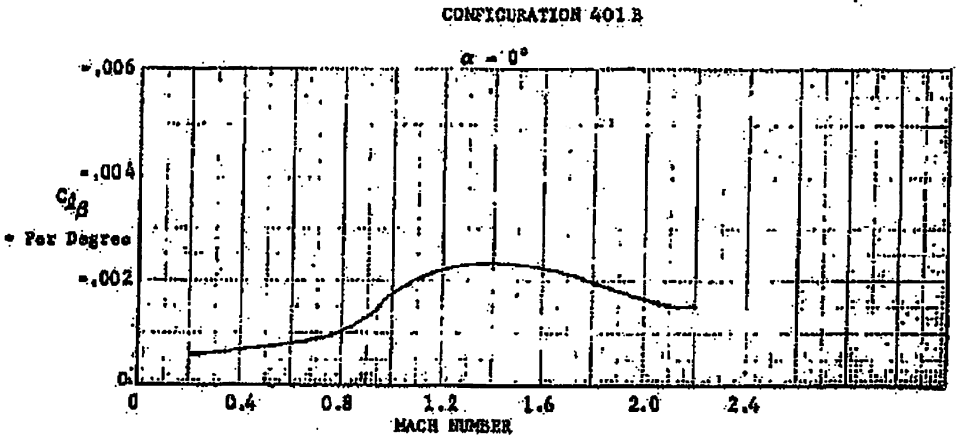

(U) Figure 3.4-11 Effective Dihedral vs Mach Number

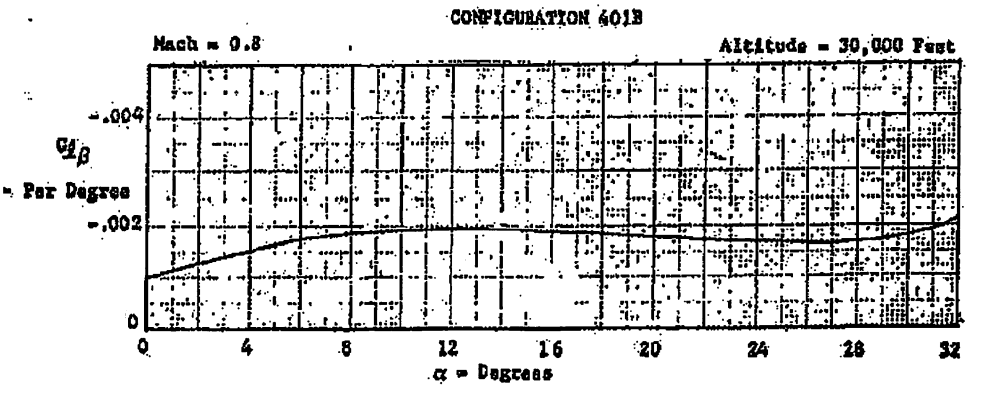

(U) Figure 3.4-12 Effective Dihedral vs Angle of Attack

(U) The variations of aileron control effectiveness with Mach number and angle of attack are shown in Figures 3.4-13 and 3.4-14, respectively. These data are based directly upon transonic roll research model tests (Reference 15). Adequate aileron control effectiveness is provided to high angles of attack. Estimated aeroelastic effects on aileron control are included and show that adequate aileron roll-control effectiveness is maintained throughout the flight envelope. The mid-wing design concept allows a highly efficient, thick, wing root structure, which, in conjunction with the low structural aspect ratio of the wing, provides a highly rigid wing airframe to preclude aeroelastic aileron roll reversal.

(U) The predicted yaw due to aileron deflection, compatible with the roll effectiveness predictions, is presented as a function of Mach number in Figure 3.4-15 and as a function of angle of attack in Figure 3.4-16. These predicted parameters are based on the results of analyses of available test data for similar configurations. The primary configuration effects were isolated and the values were estimated for the 401B arrangement. Note, particularly, that $C_{n_{\delta_a}}$ demonstrates a relatively small variation with angle of attack and does not assume very large adverse or proverse levels even at very high flight attitudes.

(U) Rudder effectiveness is presented as a function of Mach number in Figure 3.4-17. Aeroelastic effects on rudder effectiveness are based on FX estimates. Adequate directional control is available throughout the Mach-altitude flight envelope.

(U) Estimates of yaw- and roll-rate damping parameters are presented as a function of Mach number in Figures 3.4-18 and 3.4-19, respectively. These parameters are used in establishing the lateral-directional free-airplane dynamics.

3.4.4 Handling Qualities

(U) A limited analysis of the free airplane handling qualities of configuration 401B fighter has been conducted. In some cases, appropriate MIL-F-8785B specifications are indicated for comparative purposes.

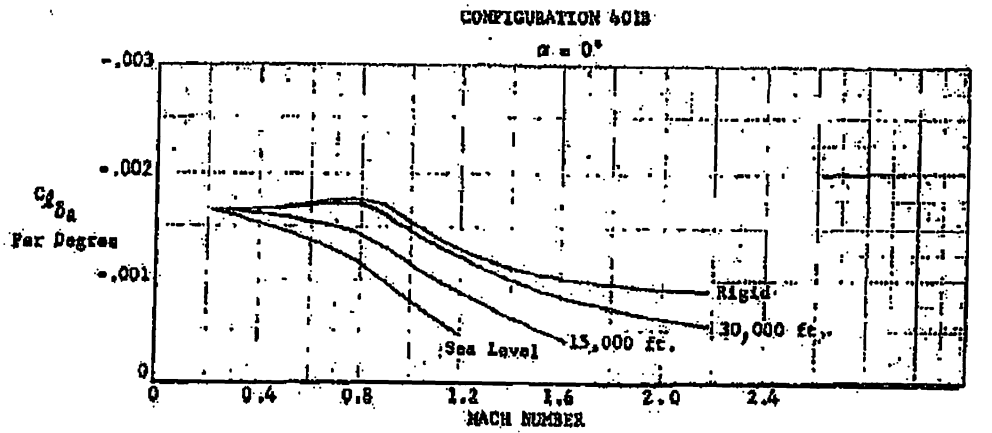

(U) Figure 3.4-13 Aileron Control Effectiveness vs Mach Number

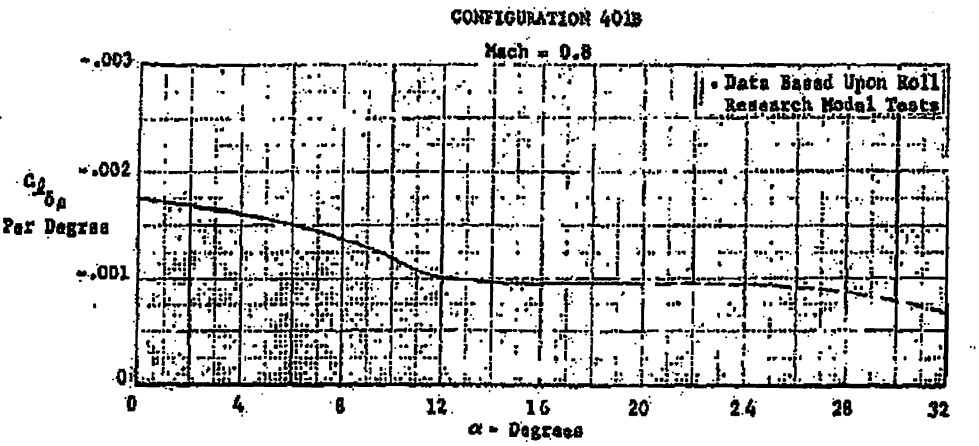

(U) Figure 3.4-14 Aileron Control Effectiveness vs Angle of Attack

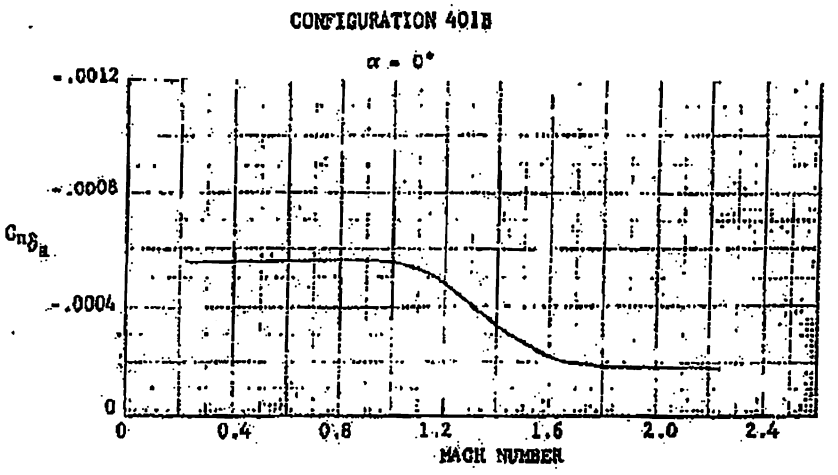

(U) Figure 3.4-15 Yaw Moment Due to Aileron Deflection vs Mach Number

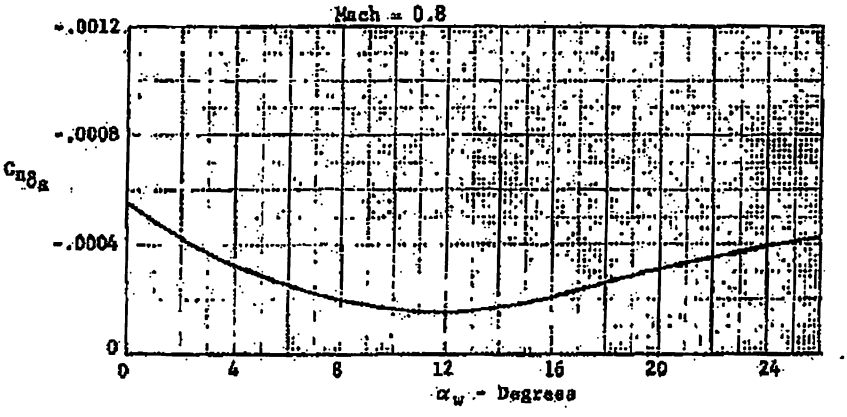

(U) Figure 3.4-16 Yaw Moment Due to Aileron Deflection vs Angle of Attack

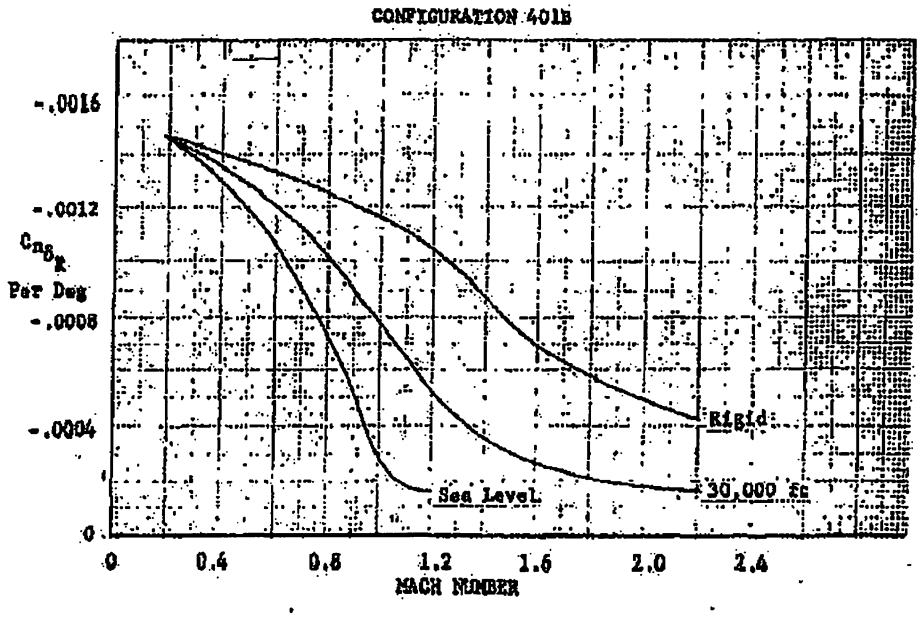

(U) Figure 3.4-17 Rudder Effectiveness vs Mach Number

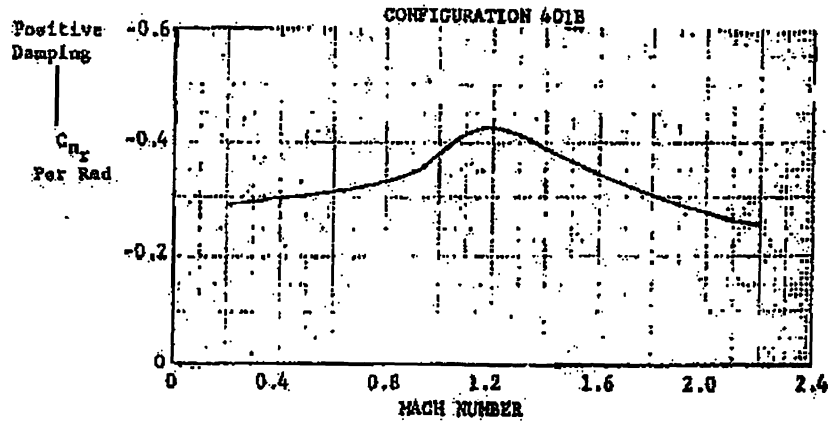

(U) Figure 3.4-18 Yaw-Rate Damping vs Mach Number

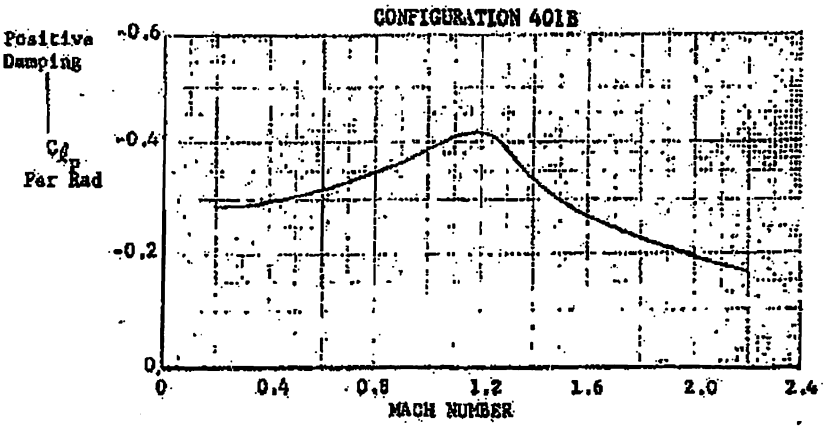

(U) Figure 3.4-19 Roll-Rate Damping vs Mach Number

(U) Pertinent handling qualities for the primary operating conditions in the combat region, shown in Figure 3.4-20, have been investigated to establish the predicted combat flight characteristics of the free airplane. These characteristics will be enhanced by a simple stability and command augmentation system.

(U) In general, the handling qualities characteristics have been investigated at the more demanding maximum sustained load factors in turning flight rather than for trim level flight. Handling qualities investigations included free-airplane longitudinal and lateral-directional dynamics, maximum trim lift, maneuver-gradients roll response, and spin-resistance factors. These analyses assumed maximum internal fuel and minimum static margin. Specific airplane parameters used are listed in Table 3.4-3. The moments of inertia are about the principal axes and the inclination of the principal axis with the wing root reference chord is 1 degree down.

~~(S)~~ Table 3.4-3 PHYSICAL PARAMETERS (U)

Gross Weight	16,800 lb
Center of Gravity	25 - 27% MAC
Pitch Inertia	31,886 slug-ft^2
Yaw Inertia	36,228 slug-ft^2
Roll Inertia	6,727 slug-ft^2
Wing Ref. Area	280 ft^2
MAC	133 in.
Wing Ref. Span	29 ft

3.4.4.1 Dynamics

(U) Longitudinal short-period frequency characteristics are presented in Figure 3.4-21 for the free airplane. Requirements of MIL-F-8785B are indicated for comparative purposes only to show that all of the combat flight conditions investigated fall in the satisfactory Level 1 region. Unaugmented short-period pitch-damping ratios for the corresponding flight conditions are tabulated in the legend in Figure 3.4-21. Good free-airplane damping ratios are evident; however, the augmentation system will further enhance these characteristics. These data are indicative of the excellent longitudinal short-period dynamic characteristics inherently designed into the 401B fighter.

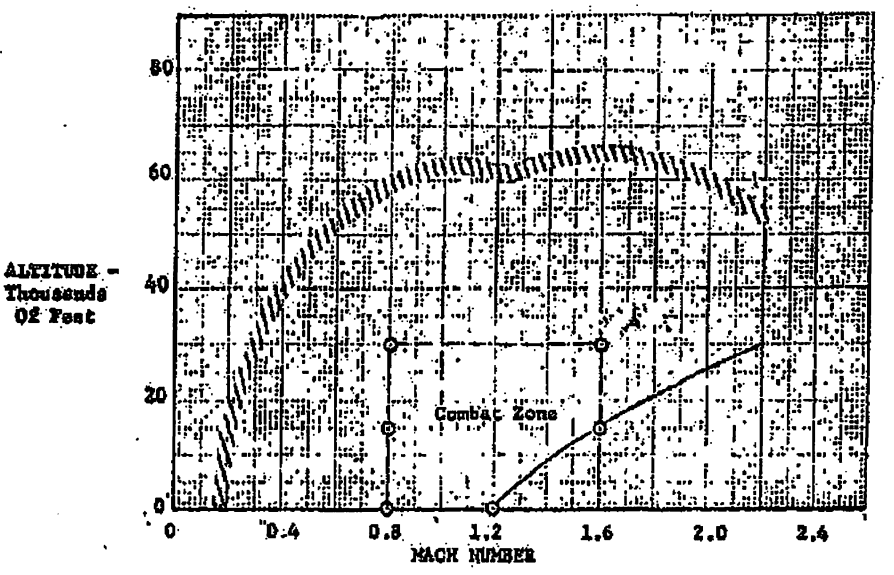

(U) Figure 3.4-20 Combat Flight Conditions

Symbol	Mach	Altitude	ζ_{sp}
x	0.8	30,000 ft	.31
⊗	1.6	30,000 ft	.15
○	0.8	15,000 ft	.41
△	0.8	Sea Level	.51
□	1.2	Sea Level	.31
◇	1.6	15,000 ft	.19

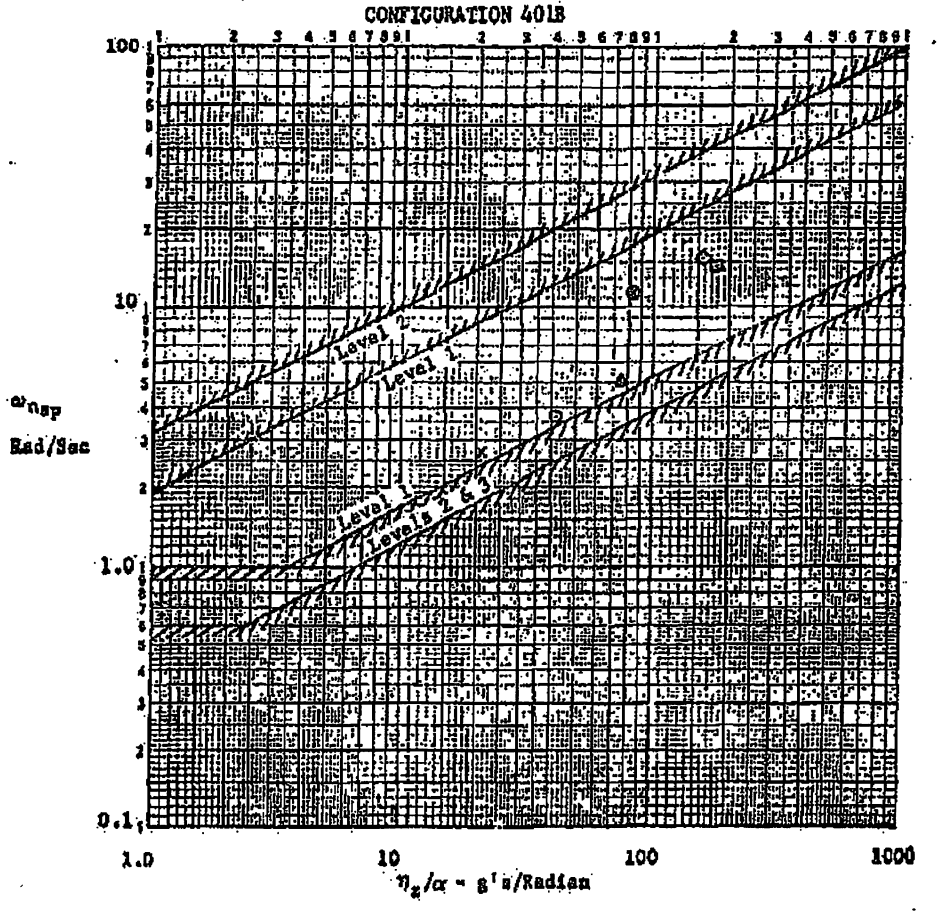

(U) Figure 3.4-21 Free-Airframe Longitudinal Dynamics

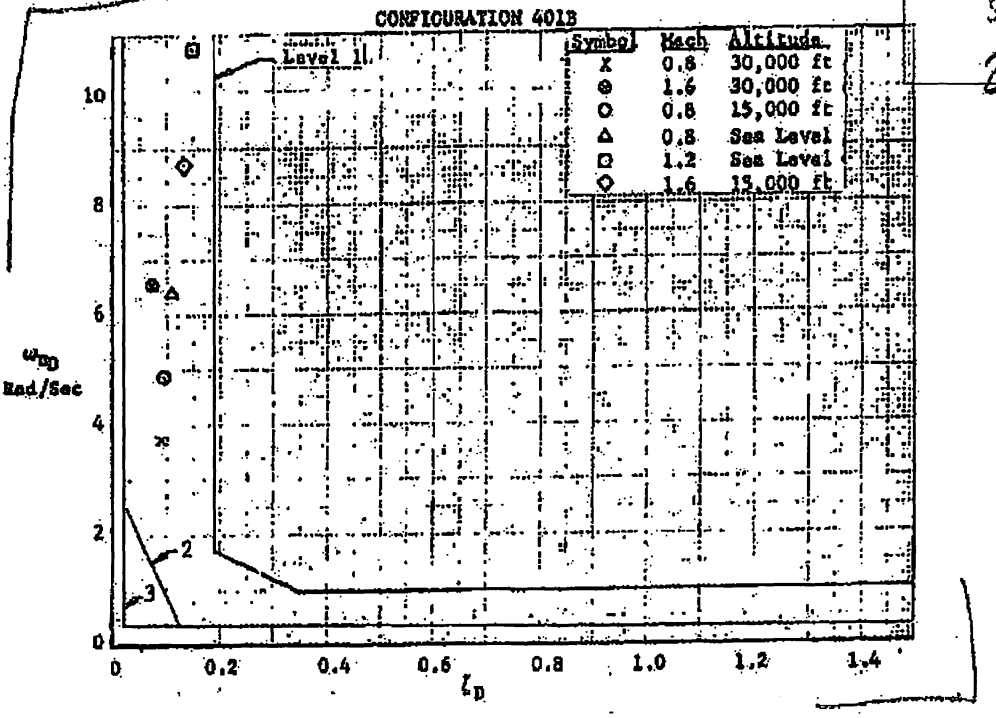

(U) Figure 3.4-22 Free-Airframe Dutch-Roll Characteristics

(U) Free airplane Dutch roll frequency as a function of damping ratio is presented in Figure 3.4-22. MIL-F-8785B requirements for Category A (combat) flight phase are superimposed for reference purposes. The analyzed flight conditions fall in the Level 2 requirements region. Level 2 represents handling qualities adequate to accomplish the mission but with some increase in work load. Consequently, achievement of Level 2 lateral-directional dynamics with the free airplane demonstrates the results of the same careful design that produced the good longitudinal dynamics. In both longitudinal and lateral-directional modes, the final augmented handling qualities of Configuration 401B will be further enhanced by the stability and command augmentation system.

3.4.4.2 Trim Control Power

(U) An all-movable horizontal tail surface is used to maximize control effectiveness at supersonic speed. Based upon an inflight aft c.g. of 27% MAC, adequate longitudinal maneuvering-response control power is available as demonstrated by the trim capability summarized in Table 3.4-4. Trim deflections have also been estimated to establish trim drag polars for the performance analysis in Subsection 3.4.

Table 3.4-4 TRIM ELEVATOR FOR LIMIT LOAD FACTOR

Alt. (ft)	Mach	$(C_L)_{n_L}$	$\delta_{H_{n_L}}$ (deg)
30,000	.8	1.3	-6.5
30,000	1.6	.326	-6.8

The trim deflections noted above have been estimated for a typical combat wing loading.

(U) Combat maneuver criteria dictate good handling qualities up to the maximum wing angle of attack as determined by aerodynamic stall or airframe structural limits. Trim lift characteristics at the Mach 0.8, 30,000-foot condition are presented in Figure 3.4-23. The pitch control power is sufficient to develop angles of attack corresponding to the maximum lift capability of the airplane within the operational envelope. Reference to Figure 3.4-10 shows that a

~~SECRET~~

CONFIGURATION 401B

Mach = 0.8
Altitude = 30,000 Feet
Gross Weight = 15,870 lbs.
Center of Gravity = 27% MAC
δ_{LEF} = 15 Degrees

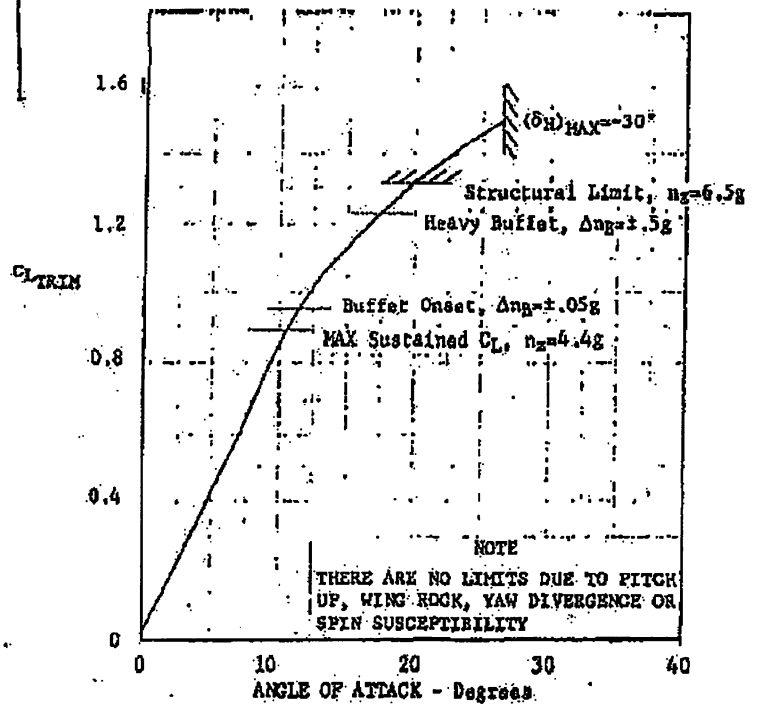

~~(S)~~ Figure 3.4-23 Trimmed Lift Curve (U)

~~SECRET~~

good level of static directional stability is maintained throughout this angle-of-attack range. Further, as discussed below in Subsection 3.4.4.5, in the dynamic directional stability and the lateral control spin parameter demonstrate high positive levels at the high angles of attack that can be developed. These positive values preclude yaw divergence and indicate the presence of high spin resistance.

3.4.4.3 Maneuver Gradients

(U) Elevator maneuver gradients (δ_H/g) have been estimated for the combat flight conditions and are listed in Table 3.4-5.

Table 3.4-5 ELEVATOR MANEUVER GRADIENTS

GW = 16,800 lb CG @ 25% MAC

Mach	Altitude (ft)	δ_H/g (deg/g)
.8	SL	- .26
.8	15,000	- .49
.8	30,000	- .90
1.2	SL	- .34
1.6	15,000	- .58
1.6	30,000	-1.11

During flight on the deck, the maneuver gradients are relatively low. Design of a command augmentation system will mask the effects of low δ_H/g values from the pilot and provide near constant stick force per g characteristics. Also, the stick force gradient (F_H/g) supplied by the pitch command augmentation below 6 g will be designed for 3 to 5 lb/g with a nearly constant relationship. In addition, the stick force gradient will be increased above 6 g to three times the normal value.

3.4.4.4 Roll Response

(U) The 401B fighter is highly responsive to pilot roll command as evidenced in Table 3.4-6 by the bank angles achieved in 1 second for full stick throw at the combat

flight conditions. The roll response quoted in Table 3.4-6 is representative of the unaugmented flexible airplane and indicates ample roll-control power availability. A roll-control command augmentation system can be incorporated to moderate the exceedingly high roll rates above 200 degrees per second and will tend to hold constant response with varying dynamic pressures.

(U) As mentioned previously, the mid-wing placement in conjunction with the low structural-wing aspect ratio affords a relatively rigid structural wing frame. This allows ailerons to be used throughout the flight envelope without encountering aeroelastic roll reversal.

Table 3.4-6 FREE-AIRPLANE ROLL RESPONSE

GW = 16,800 lb CG @ 25% MAC

Mach	Altitude (ft)	Bank Angle in 1 Second (deg)
.8	SL	168
.8	15,000	199
.8	30,000	196
1.2	SL	101
1.2	15,000	269
1.2	30,000	161

3.4.4.5 Spin Resistance

(U) Two important parameters that are prime indicators of spin susceptibility (or degree of spin resistance) are the dynamic-directional-stability parameter and the lateral-control spin parameter (LCSP). Each has been evaluated at the Mach 0.8, 20,000-foot condition and are presented as a function of angle of attack in Figure 3.4-24. Increasing positive values of these two parameters are representative of increasing spin resistance. The curves of Figure 3.4-24 indicate that positive levels are maintained to very high angles of attack. Such levels indicate that there will be a high spin resistance and that there will be no post-stall yaw departure. Thus, the fighter pilot can maneuver the 401B configuration to its maximum potential with full confidence that it has no pitch up or yaw divergence and is highly spin resistant.